












CHEMampere: Technologies for sustainable chemical production with renewable electricity and CO₂, N₂, O₂, and H₂O

Elias Klemm¹  | Carlos M. S. Lobo¹  | Armin Löwe¹  |
Verena Schallhart²  | Stephan Renninger³ | Lara Waltersmann⁴  |
Rémi Costa⁵  | Andreas Schulz⁶ | Ralph-Uwe Dietrich⁵  |
Lukas Möltner²  | Vera Meynen⁷  | Alexander Sauer^{4,8}  |
K. Andreas Friedrich^{5,9} 

¹Institute of Technical Chemistry, University of Stuttgart, Stuttgart, Germany

²Management Center Innsbruck, Innsbruck, Austria

³Institute for Photovoltaics, University of Stuttgart, Stuttgart, Germany

⁴Fraunhofer-Institute for Manufacturing Engineering and Automation, Stuttgart, Germany

⁵German Aerospace Center, Institute of Engineering Thermodynamics, Stuttgart, Germany

⁶Institute of Interfacial Process Engineering and Plasma Technology, University of Stuttgart, Stuttgart, Germany

⁷Laboratory of Adsorption and Catalysis, Department of Chemistry, University of Antwerp, Wilrijk, Belgium

⁸Institute for Energy Efficiency in Production, University of Stuttgart, Stuttgart, Germany

⁹Institute of Building Energetics, Thermal Engineering and Energy Storage, University of Stuttgart, Stuttgart, Germany

Correspondence

Elias Klemm, Institute of Technical Chemistry, University of Stuttgart, 70569, Stuttgart, Germany.

Email: elias.klemm@itc.uni-stuttgart.de

Funding information

Bundesministerium für Bildung und Forschung, Grant/Award Numbers: 01DR18002, 033RC023E, 03SF0580A, 03SFKE20-2; Bundesministerium für Wirtschaft und Energie, Grant/Award Numbers: 03EIV161A, 03ET1379A, 03ET1642D; Fonds Wetenschappelijk Onderzoek, Grant/Award Numbers: K801621N, S001619N; Horizon 2020 Framework Programme, Grant/Award Number: 763911; Ministerium für Umwelt, Klima und Energiewirtschaft Baden-Württemberg, Grant/Award Number: BWDU20101

Abstract

The chemical industry must become carbon neutral by 2050, meaning that process-, energy-, and product-related CO₂ emissions from fossil sources are completely suppressed. This goal can only be reached by using renewable energy, secondary raw materials, or CO₂ as a carbon source. The latter can be done indirectly through the bioeconomy or directly by utilizing CO₂ from air or biogenic sources (integrated biorefinery). Until 2030, CO₂ waste from fossil-based processes can be utilized to curb fossil CO₂ emissions and reach the turning point of global fossil CO₂ emissions. A technology mix consisting of recycling technologies, white biotechnology, and carbon capture and utilization (CCU) technologies is needed to achieve the goal of carbon neutrality. In this context, CHEMampere contributes to the goal of carbon neutrality with electricity-based CCU technologies producing green chemicals from CO₂, N₂, O₂, and H₂O in a decentralized manner. This is an alternative to the e-Refinery concept, which needs huge capacities of water electrolysis for a centralized

This is an open access article under the terms of the [Creative Commons Attribution](https://creativecommons.org/licenses/by/4.0/) License, which permits use, distribution and reproduction in any medium, provided the original work is properly cited.

© 2022 The Authors. The *Canadian Journal of Chemical Engineering* published by Wiley Periodicals LLC on behalf of Canadian Society for Chemical Engineering.

CO₂ conversion with green hydrogen, whose demand is expected to rise dramatically due to the decarbonization of the energy sector, which would cause a conflict of use between chemistry and energy. Here, CHEMampere's core reactor technologies, that is, electrolyzers, plasma reactors, and ohmic resistance heating of catalysts, are described, and their technical maturity is evaluated for the CHEMampere platform chemicals NH₃, NO_x, O₃, H₂O₂, H₂, CO, and C_xH_yO_z products such as formic acid or methanol. Downstream processing of these chemicals is also addressed by CHEMampere, but it is not discussed here.

KEYWORDS

catalyst ohmic heating, CO₂ utilization, electrolyzers, plasma, TRL evaluation

1 | INTRODUCTION

The Paris Climate Agreement, adopted by 196 parties on 12 December 2015, has set the goal of limiting global warming to well below 2°C, compared to pre-industrial levels. On 8 October 2018, the Intergovernmental Panel on Climate Change (IPCC) released its Special Report detailing the impacts of global warming by 1.5°C above pre-industrial levels (SR1.5).^[1] The report clearly showed that exceeding this 1.5°C global warming level by additional warming of just 0.5°C will cause tremendous damage to the ecosystems, for example, oceans, water, and land resources, and their biodiversity. Furthermore, in the report, mitigation pathways compatible with global warming of 1.5°C were given, all of which imply achieving carbon neutrality by 2050. This is a truly challenging goal considering a population growth of 1.1% per year.^[2] Depending on the magnitude and duration of a possible temporary overshoot of the 1.5°C mitigation pathway target, carbon dioxide removal from air and CO₂ sequestration will have to be performed after 2050.^[3]

Given the importance of achieving carbon neutrality by 2050, a Climate Ambition Alliance^[4] (consisting of 73 countries plus the EU, 398 cities, and 786 companies) was formed in Madrid during the UN Climate Change Conference COP25 in December 2019, which will work towards achieving net-zero CO₂ emissions by 2050 following the IPCC's SR1.5 guidelines.^[5] Countries such as Canada and Germany, the European Union, cities such as Toronto or Berlin, and companies such as SkyPower (Canada) and Beiersdorf AG (Germany) are among the members of the alliance.

The worldwide global fossil CO₂ emissions amounted to 35.6 ± 1.8 Gt in 2019.^[6] This number was expected to decline by at least 4% and as much as 7% in 2020 but only as a result of the COVID-19 pandemic.^[7] According to the *Tracking Clean Energy Progress Report 2020* on Chemicals of the International Energy Agency, direct CO₂ emissions of the chemical industry amounted to

880 Mt in 2018,^[8] which corresponds to nearly 2.5% of the global fossil CO₂ emissions (compared to the total emissions in 2019). Direct CO₂ emissions comprise the process and energy-related emissions. However, when considering the indirect CO₂ emissions as well, which account for the total carbon content of the chemical products that can be released into the environment as the product degrades over time, additional CO₂ emissions of similar amounts can be expected^[9] and the contribution of the chemical industry to the worldwide CO₂ emissions rises to 5%. In countries with a strong chemical sector, like Germany, the share of the chemical industry's CO₂ emissions to the national CO₂ emissions is higher. For instance, in Germany, the sum of the process-, energy-, and product-related CO₂ emissions of the chemical industry, that is, direct and indirect CO₂ emissions, was expected to be around 112.8 Mt in 2020^[9] (a value that is likely not to have been reached, due to the COVID-19 pandemic), which would have corresponded to 16% of the total 702 Mt of CO₂ emitted in Germany,^[10] while in Canada, for example, which does not have such a strong chemical industry, this value was 6.8 Mt of CO₂, out of a total of 730 Mt of CO₂ emitted in 2019.^[11]

To achieve the goals set by the UN Climate Change Conference in 2019, all industrial sectors, including the chemical industry, have to achieve net-zero CO₂ emissions by 2050. Highly industrialized countries such as Germany or Canada have major responsibilities to develop fundamentally new technologies and processes for a CO₂-neutral chemical production. Aside from enhanced chemical recycling of waste and a shift towards biomass as a raw material (bioeconomy), CO₂ itself can be used as a carbon source to produce hydrocarbons. Thus, by also collecting CO₂ from the air by direct air capture processes in the long-term future^[12,13] or from biobased processes such as biogas or bioethanol production and biomass power plants (a concept known as integrated biorefinery^[14]) in the medium-term future, the carbon cycle can be closed.

During this transition to a chemical production with net-zero CO₂ emissions, such emissions can be mitigated, in the short-term future, by reusing the CO₂, which is formed as a waste product in fossil-based processes such as steel, cement, ammonia, or ethylene oxide production, to mention some of the largest contributors of industrial CO₂ emissions.^[15–17] This can, at the very least, reduce the overshoot of the 1.5°C mitigation pathway target and thus the effort for carrying out net-negative emissions, that is, irreversibly removing CO₂ from the atmosphere. However, chemicals and their corresponding products contain not only H and C atoms but also heteroatoms such as O and N as the most prominent ones, all of which can be found in the air, making it an ubiquitous raw material that is readily available. The availability of water as a hydrogen source is not as unlimited as one might think, and its availability depends on geographical, economic, and social factors. Figure 1 visualizes the material flow of a CO₂-neutral chemical industry using air and water as resources instead of oil, gas, and coal, by a tree with aerial roots.

To become completely CO₂ neutral, the energy demand of the whole chemical production process must be supplied by renewable sources such as hydro, solar, wind, tidal, geothermal, etc. Processes using solar power to drive chemical reactions (photochemistry) can be considered to be artificial or technical photosynthesis, but while such a concept might be highly attractive, its main

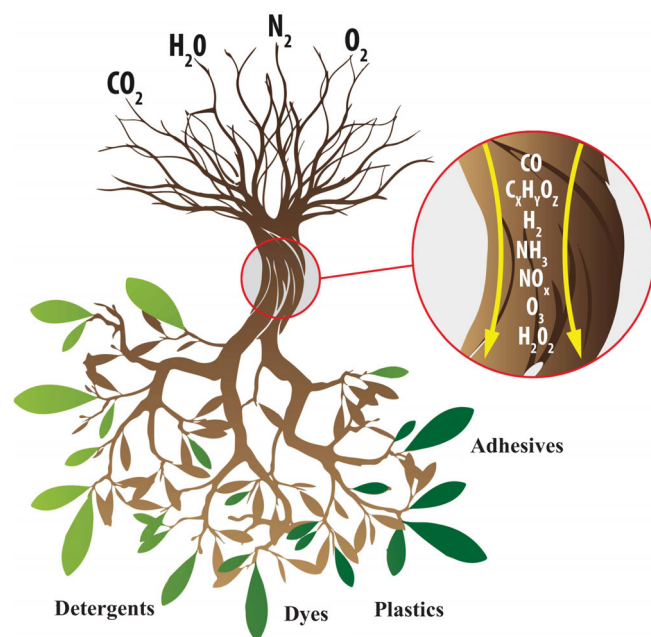


FIGURE 1 New “ChemisTree” with aerial roots as an illustration of the value-added supply chain from air and water as raw materials to some selected important end products whose respective industries, combined, are expected to be worth at least 900 billion US dollars, worldwide, by 2026^[18–21]

drawback is that this process is completely reliant on a single energy source, which supplies a variable amount of energy throughout the day, making continuous production challenging, particularly in developed countries, which, in general, tend not to be the best geographically placed to make the best use of solar energy. Thus, this technology is still in its infancy and needs to be pushed to higher technology readiness levels (TRLs) before it can be successfully implemented on an industrial scale. In contrast, a larger share of processes that activate CO₂, N₂, O₂, and H₂O with the help of electricity generated from renewable primary energy sources are already at higher TRLs and closer to industrial application. These processes have the advantage of being able to make use of several different renewable energy sources, which allow them to be used in a wider array of geographical locations with continuous operation. Of course, complete CO₂ neutrality means that electricity from renewable sources must be used in all other upstream and downstream process units as well. In essence, this leads to an “all-electric” process, which needs to be highly heat integrated, because electrical processes always lead to some degree of Joule heating effect, which is hard to avoid. Thus, special attention has to be paid to heat recovery, heat storage, and heat transfer, for example, using heat pumps, to further increase the efficiency of the processes.

The amount of renewable energy available at present is too low to power all human activities.^[9] Therefore, heat recovery, especially at lower temperature levels, is mandatory if the energy is to be used efficiently. This leads to the concept of an ultra-efficient¹ factory, which is defined as a loss-free production site, which has a positive symbiotic relationship with its environment.^[22] Aiming at a holistic view of production sites, the concept of the ultra-efficient factory follows five fields of action, namely, material, energy, emission, human/staff, and organization.^[23,24] Thus, the electrification of the chemical industry, in combination with efficient heat recovery, is one of the keys to reach the concept of an ultra-efficient chemical factory.^[25]

Due to the large electricity requirements of industrial processes, those regions of the world with a high potential for wind and solar energy production are preferred to host such ultra-efficient chemical factories. For example, regions with a high potential for solar energy production are the so-called sun-belt regions of the world, namely, the Mediterranean Area, Northern Africa, South Africa, China, India, Latin America, and Australia. It can be expected that chemical production based on electricity from renewable sources and CO₂, N₂, O₂, and H₂O as raw materials will become economically competitive first for speciality chemicals (Power-2-Specialities) and afterwards for commodities (Power-2-Commodities).^[26] The decentralized production of not

only the specialty chemicals but also of the final products seems to be practicable both from a technological as well as from an economic point of view.^[26]

CHEMampere² is a research initiative of the University of Stuttgart (Germany) with the goal of investigating and developing electrically driven technologies to utilize CO₂, H₂O, N₂, and O₂ as raw materials and produce final products such as adhesives, detergents, dyes, and plastics in an ultra-efficient chemical factory. CHEMampere will address greenhouse gas neutrality of the whole process, including upstream and downstream processing and heat integration. The core reactor technologies of CHEMampere for using electricity from renewable sources to drive chemical reactions have been chosen to be electrolysis, plasma, and ohmic resistance heating of catalysts (see Figure 2).

As can be seen from Figure 1, the intermediates accessible from the CHEMampere reactor technologies are NH₃, NO_x, O₃, H₂O₂, H₂, CO, and C_xH_yO_z such as formic acid, methanol, ethanol, ethylene, or propanol. These are the platform chemicals of an electricity-based chemical industry using CO₂, air, and water as raw materials, similar to the typical platform chemicals of a bio-based circular economy such as ethanol, furfural, or hydroxymethylfurfural,^[27] which will also significantly contribute to future CO₂-neutral chemical production. Even combinations of the two concepts are promising, for example, using platform chemicals from electricity-driven technologies such as formic acid or synthesis gas³ (syngas) for microbial fermentation to produce value-added products such as isobutylene, crotonic acid, polyhydroxybutyrate, butanol, and hexanol.^[28,29]

CHEMampere follows the concept of decentralized and distributed production, given the fact that renewable electricity production is itself often decentralized and that the largest renewable electricity power plants are capable of producing electricity in the order of several gigawatts

(GW). Thus, building a centralized eRefinery that is based on green mega-methanol or Fischer–Tropsch plants utilizing green hydrogen from water electrolysis and CO₂ would require hundreds of GW of renewable power plants to be feasible. Nevertheless, such chemical routes will significantly contribute to the CO₂-neutral production of chemicals in the mid-to-long-term future.^[30] However, less integrated, decentralized plants are also needed for the CO₂-neutral dedicated production of certain intermediates and products, as discussed in this article. Naturally, decentralized plants cannot take advantage of the economy of scale, which is typical for the aforementioned chemical routes, thus making them less profitable for small-scale production. However, the direct conversion towards the target products, as described in this article, would avoid the dependence on green hydrogen from water electrolysis, which is desired because green hydrogen will also be demanded in large quantities by the energy sector. In any case, technology diversity is needed for future chemical production because, at this point, no one can anticipate to what extent each technology will contribute to CO₂-neutral chemical production, such as, for example, technologies for a circular bioeconomy, for a methanol economy, for chemical recycling, and for decentralized production with renewable electricity as described in this article. Moreover, local differences in resource availability, supply chains, industrial activities, and policies, for example, can also influence the choice of the most suitable process.

The present review focuses on the electricity-driven core reactor technologies shown in Figure 2 (electrochemistry, plasma, and ohmic resistance heating). Their state of the art is described, the advantages/disadvantages are discussed, and research needs are identified. TRLs are evaluated with regard to the conversion of CO₂, N₂, O₂, and H₂O to the intermediates NH₃, NO_x, O₃, H₂O₂, H₂, CO, and C_xH_yO_z. Thus, the processes from the intermediates towards the final

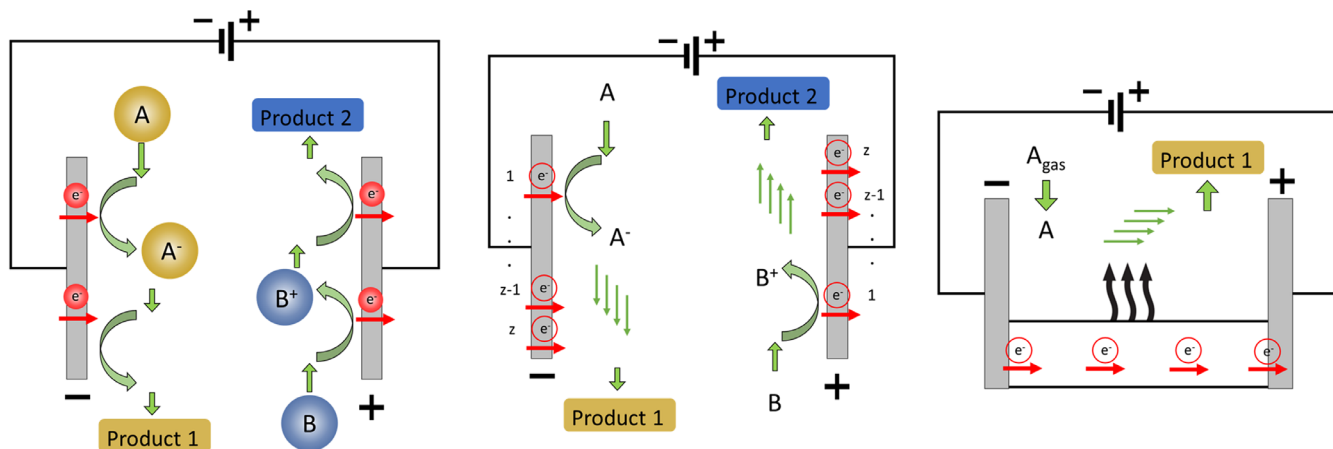


FIGURE 2 Electricity-driven core reactor technologies of CHEMampere. Left: Electrochemical processes; centre: Plasma-based processes; and right: Ohmic resistance heating of catalysts

products lie outside the scope of this publication and are not discussed here, but a general consideration of the efficiency of chemical production with renewable electricity is discussed.

2 | TECHNOLOGIES USED IN CHEMAMPERE

2.1 | Electrolysis

2.1.1 | Low-temperature electrolysis

Low-temperature electrolysis occurs, as one might expect, at temperatures within the range of liquid water (i.e., below 100°C) and usually at a pressure equal to (or close to) atmospheric pressure. Some processes, like low-temperature water electrolysis (LT-WEL), which operate between 60–80°C,^[31] are already at a quite mature stage, that is, already commercialized.^[32] Others, such as low-temperature CO₂-H₂O, N₂-H₂O, or O₂-H₂O-electrolysis (LT-CO₂EL, LT-N₂EL, and LT-O₂EL), which operate between 20–50°C,^[33] are still at a lower TRL level. The

reduction reactions of the different electrolysis processes, in both alkaline and acidic conditions, as well as the oxygen evolution reaction (OER), which is usually the anodic reaction in all cases, are given in Table 1 along with their respective equilibrium potentials.

Existing cell configurations

To perform the reactions mentioned above, a variety of different cell concepts have been presented in the literature. Within CHEMampere, focus is placed on those concepts that make use of: (1) gas diffusion electrodes (GDEs) to enhance the mass transport of gaseous reactants or products towards and away from the reaction zone for achieving high current densities^[34] and (2) ion-exchange membranes that can either be a cation exchange membrane (CEM) or an anion exchange membrane (AEM) or even both, to avoid product crossover to and losses at the anode.^[35,36] The remainder of Section 2 is dedicated to exploring the advantages and disadvantages of each of the designs as well as their suitability for CHEMampere-related processes. In principle, unless stated otherwise, these cell configurations can be adapted to all of the above-mentioned electrolysis processes.

Reduction reactions		Equilibrium potential (V vs. SHE)	
Acidic conditions (pH = 0)			
$N_2 + 6H^+ + 6e^-$	\rightleftharpoons	$2NH_3$	+0.06 (I)
$O_2 + 2H^+ + 2e^-$	\rightleftharpoons	H_2O_2	+0.62 (II)
$2H^+ + 2e^-$	\rightleftharpoons	H_2	0.00 (III)
$CO_2 + 2H^+ + 2e^-$	\rightleftharpoons	$CO + H_2O$	-0.10 (IV)
$CO_2 + 2H^+ + 2e^-$	\rightleftharpoons	$HCOOH$	-0.17 (V)
$CO_2 + 6H^+ + 6e^-$	\rightleftharpoons	$CH_3OH + H_2O$	+0.02 (VI)
$2CO_2 + 12H^+ + 12e^-$	\rightleftharpoons	$C_2H_5OH + 3H_2O$	+0.08 (VII)
$2CO_2 + 12H^+ + 12e^-$	\rightleftharpoons	$C_2H_4 + 4H_2O$	+0.08 (VIII)
$3CO_2 + 18H^+ + 18e^-$	\rightleftharpoons	$C_3H_7OH + 5H_2O$	+0.11 (IX)
Alkaline conditions (pH = 14)			
$N_2 + 6H_2O + 6e^-$	\rightleftharpoons	$2NH_3 + 6OH^-$	-0.77 (X)
$O_2 + 2H_2O + 2e^-$	\rightleftharpoons	$H_2O_2 + 2OH^-$	-0.21 (XI)
$2H_2O + 2e^-$	\rightleftharpoons	$H_2 + 2OH^-$	-0.83 (XII)
$CO_2 + H_2O + 2e^-$	\rightleftharpoons	$CO + 2OH^-$	-0.93 (XIII)
$CO_2 + H_2O + 2e^-$	\rightleftharpoons	$HCOO^- + OH^-$	-0.69 (XIV)
$CO_2 + 5H_2O + 6e^-$	\rightleftharpoons	$CH_3OH + 6OH^-$	-0.81 (XV)
$2CO_2 + 9H_2O + 12e^-$	\rightleftharpoons	$C_2H_5OH + 12OH^-$	-0.75 (XVI)
$2CO_2 + 8H_2O + 12e^-$	\rightleftharpoons	$C_2H_4 + 12OH^-$	-0.75 (XVII)
$3CO_2 + 13H_2O + 18e^-$	\rightleftharpoons	$C_3H_7OH + 18OH^-$	-0.72 (XVIII)
Oxidation reactions			
Acidic conditions (pH = 0)			
$2H_2O$	\rightleftharpoons	$O_2 + 4H^+ + 4e^-$	+1.23 (IXX)
Alkaline conditions (pH = 14)			
$4OH^-$	\rightleftharpoons	$O_2 + 2H_2O + 4e^-$	+0.40 (XX)

TABLE 1 CHEMampere intermediates that can be produced directly from CO₂, N₂, O₂, and H₂O by low-temperature electrolysis under alkaline or acidic electrolyte conditions

Cell design using a cation exchange membrane

The first design to be explored is the cell design using a CEM, which is the most prominent design, mainly due to its high chemical stability and acceptable ohmic resistance. Although they are often associated with an acidic environment, like in the well-known acidic proton exchange membrane water electrolysis (PEMWEL), CEMs can also be employed when alkaline liquid electrolytes are required. Such a cell configuration is shown in Figure 3A.

In alkaline CEM-based cells, hydroxide ions are produced at the cathode, according to Equations (X)–(XVIII) in Table 1, but they are prevented from reaching the anode by the CEM. Instead, cations (e.g., potassium) that are leftover from hydroxide consumption at the anode move through the membrane to the cathode side to maintain charge neutrality in the cell. In the case of LT-CO₂EL, the CEM thereby effectively prevents the oxygen produced at the anode from being contaminated with CO₂ due to bicarbonate crossover from the cathode side. Furthermore, the alkaline anodic environment generally allows for the use of non-precious metal catalysts like nickel or iron-based systems and cheaper bipolar plate materials like stainless steel. However, this configuration comes with the downside of an unstable pH value. The anode pH gradually decreases while the cathode pH increases,^[7] making downstream pH balancing necessary.

Instead of a liquid, an anodic zero-gap configuration, incorporating a membrane electrode assembly (MEA), can be used (Figure 3B). The direct contact between anode and membrane circumvents the need for a highly conductive anolyte⁴ and allows for the use of pure water instead. Due to the lack of other metal cations, protons are transferred through the membrane, neutralizing the

hydroxide ions produced at the cathode or replenishing consumed protons. While this configuration now allows for a stable pH at the cathode,^[7] the anode's acidic environment requires the use of precious metal catalysts, like iridium, as well as corrosion-resistant cell materials.

Both the configurations described above show a severe downside when it comes to liquid or solved products, which require a liquid film to be present between the cathode and the membrane (Figure 3A,B). Even when adding large amounts of conductive salts (which can, in turn, lead to problems in the product purification steps), this film adds a significant amount of ohmic resistance and potential heat removal problems in an industrial-scale cell. This may be avoided by using a full zero-gap configuration as known from PEMWEL (Figure 3C). Avoiding the liquid electrolyte film and supplying water only by humidification or electroosmotic drag from the anode can also help to increase the concentration of liquid products. However, three major challenges arise with this configuration: first, once again, the need to use precious metals on the anode; second, products need to be removed efficiently without completely displacing the reactant; and third, the close proximity between the highly acidic membrane and cathode brings along the problem of a competing hydrogen evolution reaction (HER) for technologies except for LT-WEL.

Cell design using an anion exchange membrane

AEMs can be used analogously to what has been described for CEM-based designs (Figure 3), with the difference being that it is now anions that are transported through the membrane to close the electrical circuit. For the purposes of CHEMampere, the main drawback of this configuration is that it is not applicable to all processes listed in Table 1. While alkaline membrane water electrolysis is a

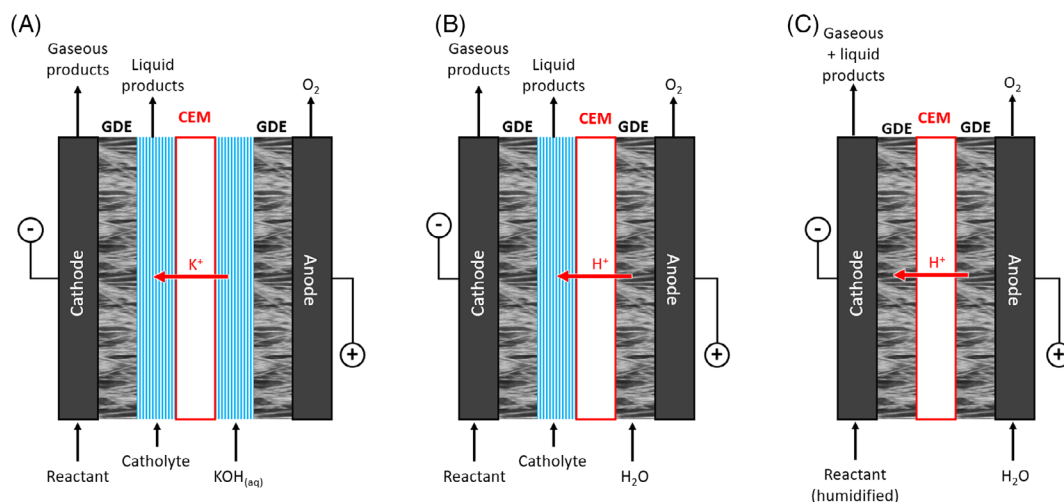


FIGURE 3 Various cation exchange membrane-based electrolyzer configurations, potentially applicable for all mentioned low-temperature (LT)-electrolysis technologies

well-known process with great advantages for stationary and steady operation, LT-CO₂EL and LT-O₂EL experience some severe disadvantages. For LT-CO₂EL, hydroxide ions formed at the cathode can react with CO₂ to reversibly form bicarbonate/carbonate ions, which then migrate to the anode (where, as mentioned before, the OER takes place), where they are once again converted to CO₂, contaminating the oxygen product stream. In the case of LT-O₂EL towards hydrogen peroxide, the existing alkaline conditions impair the product stability.

Cell design using anion and cation exchange membranes

CEM-based configurations have recently been subjected to modifications and can now incorporate both an AEM and a CEM. The membranes can either be separated (Figure 4A) or attached to each other, forming a bipolar membrane (BPM, Figure 4B). Separating the AEM and CEM, depending on the application, can prove beneficial in the following ways. First of all, since the AEM is placed over the cathode GDE, it acts as a protection layer for the catalyst, which allows the bulk electrolyte to be much more acidic than the reaction environment inside the cathode GDE. Second, the AEM can also inhibit the precipitation of salts (such as potassium bicarbonate^[37]) in the porous cathode by keeping cations in the bulk phase and facilitating anion removal, ultimately decreasing the degradation of the electrode.^[38] Lastly, if an ion-conducting resin is introduced in the electrolyte compartment, there is no need for a conducting salt to be introduced, which leads to the generation of a pure product stream,^[39] and, consequently, the overall operating costs are reduced.

As mentioned earlier, the AEM and CEM can be placed adjacent to one another, thereby forming a BPM, which results in a setup similar to the one just discussed above. With such a setup, the focus inherently shifts towards the pH values within the cell. Upon applying a

voltage, water is split inside the BPM (at a thin catalyst layer between the AEM and CEM), forming protons and hydroxide ions, which are transported to the cathode and anode, respectively. This allows the anode to be operated under alkaline conditions, while the protons delivered to the catholyte maintain pH stability. However, this water-splitting reaction adds a significant voltage drop in the system (around 1 V at 100 mA/cm²).^[40] Hence, such a cell configuration needs to be economically evaluated for each individual application to determine if the higher operating expenditures (higher cell voltage) justify the lower capital expenditures, CAPEX (cheaper catalysts and cell materials).

2.1.2 | High-temperature electrolysis

High-temperature electrolysis processes, referred to as solid oxide electrolysis (SOE), are attractive due to the possibility of attaining higher reaction rates and due to the lower specific electrical energy consumption compared to low-temperature electrolysis, given that some of the energy is supplied to the system in the form of heat.^[41] This makes the processes especially attractive if a renewable heat source is available. High-temperature electrolysis reactions typically take place at temperatures above 600°C in ceramic-based membrane reactors, which are electrochemical reactors that are especially attractive for the direct conversion of electricity into chemicals, owing to their fast kinetics.

Ceramic-based electrochemical cells can be classified into two main families depending on the nature of the charge carrier in the electrolyte material. The solid oxide cells (O-SOC) rely on ionic oxygen transport through the electrolyte while the proton conducting solid oxide cells (H-SOC), also known as proton

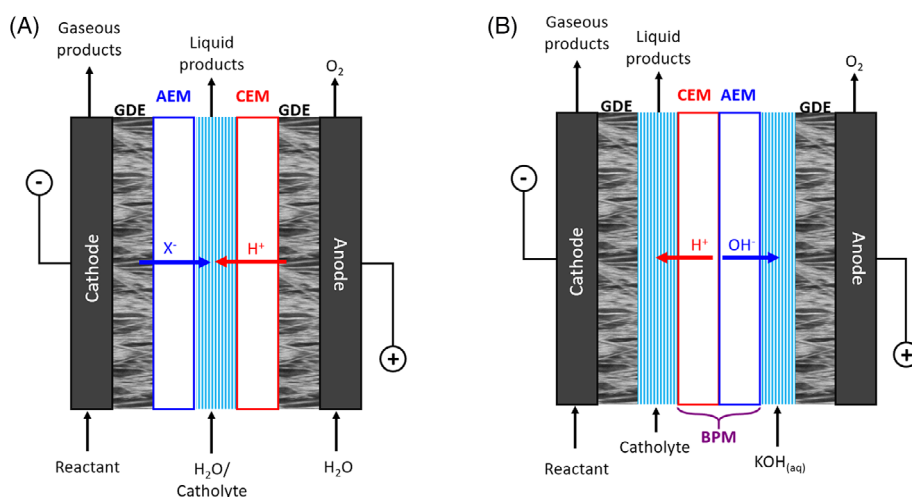


FIGURE 4 Potential cell configurations with both cation and anion exchange membranes

conducting ceramic (PCC) cells, implement a solid-state electrolyte that enables the transport of protons. By design, O-SOE is especially appropriate for oxygenation/deoxygenation reactions, whereas the proton-conducting solid oxide electrolysis (H-SOE), on the other hand, finds its application in processes that call for protonation/deprotonation reactions (see Table 2). Both of these designs will be further explored in this section.

Oxygen ion conducting solid oxide electrolysis cells (O-SOC)

O-SOC exist in multiple cell architectures, but the planar design, owing to its compactness and high specific power density, has so far received most of the attention and is by far the most commonly used architecture to develop O-SOE for commercial applications. O-SOC can be further subdivided into: (i) the so-called electrolyte supported cell (ESC) and (ii) the cathode supported cell (CSC). They are briefly discussed below.

ESC relies on a thick and dense zirconia-based electrolyte (60–200 μm), which provides sufficient mechanical strength to the cell and supports the cathode material. They are operated at high temperatures, typically above 800°C to minimize the ohmic losses related to the electrolyte thickness. As a cathode material, a Ni/Ce_{1-x}Gd_xO_{2-x} (CGO) cermet is used since it shows promising features such as a good redox stability, high coking resistance, and a fair tolerance towards potential sulphur-containing impurities in CO₂ sources^[42-47] (see also Section 2.1.3).

In the CSC design, a thick and porous cermet cathode, which is around 300 μm thick, provides the mechanical strength of the cell and supports a thin and dense zirconia-based electrolyte (5–15 μm). The cathode is typically made of a Ni/Zr_{1-x}Y_xO_{2-x} (YSZ) cermet. Compared to ESC, the thin electrolyte allows reduced ohmic losses, which improves the overall performance. Therefore, the CSC operates at a lower temperature, typically in the range of 700–800°C. However, the CSC design faces critical challenges due to the thick and porous YSZ support layer, in particular, a low tolerance towards redox and thermal cycling and a poor tolerance towards carbon deposition.

Both types of cells are especially well suited for the production of the CHEMampere-relevant products: H₂, CO, and syngas^[41,48] via steam electrolysis, dry CO₂ electrolysis, and simultaneous co-electrolysis of H₂O and CO₂ (Figure 5), for a wide range of CO/H₂ ratios.^[41,48] Moreover, they can also operate in pressurized conditions. An overview of the functionality of the different cell types in the different conditions can be found here.^[41,49-51]

High-temperature electrolysis is very attractive in terms of efficiency, for H₂ and CO production, compared to low-temperature technologies. This is even more favourable if a heat source is available to reduce the heat demand of the electrolysis process. Nonetheless, industrialization of the technology and scaling up to the multi-megawatt (MW) scale is still challenging, as SOE is CAPEX intensive compared to low-temperature

TABLE 2 CHEMampere intermediates that can be produced directly from CO₂, N₂, O₂, and H₂O by solid oxide cells (O-SOE) (O²⁻) and proton-conducting solid oxide electrolysis (H-SOE) (H⁺)

				Equilibrium cell voltage at 600°C (V) ^a	
O-SOE					
Overall	2H ₂ O	⇌	2H ₂ + O ₂	1.05	(I)
Reduction	2H ₂ O + 4e ⁻	⇌	2H ₂ + 2O ²⁻		
Oxidation	2O ²⁻	⇌	O ₂ + 4e ⁻		
Overall	2CO ₂	⇌	2CO + O ₂	1.11	(II)
Reduction	2CO ₂ + 4e ⁻	⇌	2CO + 2O ²⁻		
Oxidation	2O ²⁻	⇌	O ₂ + 4e ⁻		
H-SOE					
Overall	N ₂ + 3H ₂ O	⇌	2NH ₃ + 3/2 O ₂	1.19	(III)
Oxidation	3H ₂ O	⇌	3/2 O ₂ + 6H ⁺ + 6e ⁻		
Reduction	N ₂ + 6H ⁺ + 6e ⁻	⇌	2NH ₃		
Overall	2H ₂ O	⇌	2H ₂ + O ₂	1.05	(IV)
Oxidation	2H ₂ O	⇌	O ₂ + 4H ⁺ + 4e ⁻		
Reduction	4H ⁺ + 4e ⁻	⇌	2H ₂		

^aThermochemical data extracted from the NIST database.

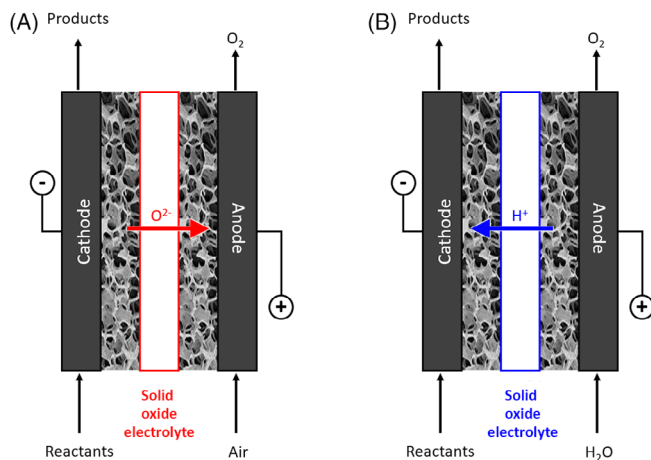


FIGURE 5 Typical configurations of high-temperature electrolysis cells. (A) Solid oxide cells (O-SOC). (B) Proton conducting solid electrolyte cells (H-SOC)

electrolysis, and the ceramic processing challenges do not allow for large cell areas. Furthermore, the dynamic response of large SOE systems to the fluctuation of renewable electricity is still challenging. Dealing with the carbon deposition during CO_2 electrolysis is still a problem, which requires material optimization to prevent metal dusting of the metallic components and safe operating strategies.

Proton conducting solid oxide electrolysis cells (H-SOC)

PCCs and related technologies are relatively young, that is, the first evidence of proton transport in ceramics was presented in 1981. Considerable progress has been made in the last decade, which has boosted the performance of laboratory-scale devices to a level suitable to consider commercialization of the technology.^[52] H-SOC were developed, and their potential application for different *Power-to-X* applications was demonstrated for reactions relevant to CHEMampere, which include steam electrolysis and direct electrosynthesis of ammonia (see Table 2). For all of these applications, PCCs provide a unique competitive solution compared to oxygen ion-conducting ceramics.^[53] Typically operating between 400 and 600°C, H-SOC are particularly promising for such applications. The electrode configuration separates steam supply and hydrogen production, thereby preventing dilution of both streams while keeping the reversibility capability (e.g., see Figure 5B). However, despite these advances, the commercialization of H-SOC is far behind other similar ceramic-based technologies such as the O-SOC. Promising state-of-the-art protonic ceramic electrolytes, for example, $BaZrCeO_3$ -based perovskites, are hard to densify, which makes it challenging to develop membrane reactors due to: (i) the

lack of scalable, cost-effective, and reliable manufacturing processes and (ii) the lack of suitable electrode materials available as they must be thermochemically compatible with other components while ensuring good catalytic activity towards the desired reaction.

By 2020, solid-state reactive sintering (SSRS) had already been broadly adopted for the production of tubular cells (CoorsTek Membrane Sciences AS, Oslo, Norway) and planar cells (FuelCell Energy Inc., USA; PANASONIC, Japan). It represents the state of the art of H-SOC manufacturing.^[54] However, despite its broad deployment, this method still faces some challenges. In particular, the incorporation of NiO as a sintering aid in the electrolyte hinders the protonic transport properties of the electrolyte and is suspected to add some electronic conductivity.^[54] Furthermore, the presence of a secondary phase can potentially lower the mechanical strength of the electrolyte over long-term operation. Moreover, since it relies on the reactivity of the electrolyte precursor with NiO to achieve the high density of the electrolyte, SSRS leaves very little flexibility in the choice of materials for the cathode, which negatively impacts the range of applications of the cells, since the materials cannot be selected for the sake of their performance. A particularly important challenge for H-SOE is the p-type leakage across the electrolyte that induces a flux of protons from the cathode to the anode side and thus strongly reduces the Faraday efficiency. The minimization of this current leakage through optimization of the electrodes, electrolyte material, cell architecture, and operating conditions is mandatory to achieve high process efficiency.

2.1.3 | Catalysts

Considering the requirement for high current densities in industrial applications, GDEs have become the state-of-the-art solution to overcome the mass transport limitation resulting from the low gaseous reactant solubility in aqueous electrolytes for LT-electrolysis. Their purpose is to provide a large surface area at which solid, liquid, and gaseous phases coexist and form the so-called triple phase boundary. As seen in chemical Equations (I)–(IX) or (X)–(XVIII) in Table 1, each of the listed reactions includes electrons, ionic species, and a gaseous reactant or product that needs to be transported. Hence, GDEs usually consist of an electrically conductive material like metals or carbon-based materials (e.g., carbon black, graphite, etc.) and solid or liquid electrolytes that provide the ability to transport ionic species. The porous structure necessary for gas transport is usually created by adding hydrophobic binders like Teflon to render the electrode (partly)

hydrophobic and prevent flooding. If not added as a conductive metal itself, the electrocatalyst is often supported on carbon or other metals (e.g., titanium) and covered with a thin film of liquid electrolyte during the cell operation, allowing the gaseous reactant to reach the active site.

Although a lot of recent and current work is focused on finding new catalyst materials for LT-electrolysis, typical elements can be named for each product. Mo-based materials are known in NH_3 synthesis,^[55] while Hg, Au, Ag, Pt, and Pd can form hydrogen peroxide.^[56] Pt, Ir, Ag, and Ni are typical for LT-WEL.^[57] LT- CO_2 EL to CO usually works well on Ag, Au, and Zn, while formate/formic acid can be produced on Sn, Bi, In, Pb, or Hg. Copper is the only element known in LT- CO_2 EL that allows the formation of alcohols or aliphatic hydrocarbons.^[58]

In HT-electrolysis, for both the O-SOC and the H-SOC, a porous nickel-based cermet has become the state-of-the-art cathode. It consists of a mixture of nickel and an oxidic phase that acts as an ionic conductor. The purpose of the nickel phase in the form of a 3D percolation network is to ensure a good current distribution in the volume of the electrode while catalysing the cathode reactions. The oxidic phase enables the transport of the ions involved in the electrochemical reaction to or from the active sites located at the so-called triple phase boundary, that is, at the junction of the nickel and the oxidic materials facing the gaseous atmosphere. When the oxidic material is a mixed ionic and electronic conductor, such as CGO in O-SOC (see Section 2.1.2), the electrode reaction is delocalized over the double-phase boundary between the oxidic and the gas phases. The microstructure of the electrode, in terms of porosity, pore size distribution, and tortuosity, is tuned to maximize the density of reactive sites while minimizing gas transport resistance.

In the specific case of O-SOC, however, it has recently been shown that, specifically for electrolysis operation, the cermet is prone to microstructural instabilities at high operating current densities, that is, at large cathodic overpotentials, in the form of Ni migration away from the electrode/electrolyte interface thus causing severe degradation.^[59–61] Moreover, traditional cermet electrodes require activation and operation within a reducing atmosphere, that is, H_2 or CO , which impedes operation under pure H_2O or pure CO_2 streams. Therefore, the development of oxidic electrocatalysts that are fully redox stable such as perovskite materials would be beneficial to enable their operation under pure H_2O or pure CO_2 streams, which could result in a system simplification and thus cost reduction.

In the specific case of H-SOC, the anode materials remain an important challenge. Recently, mixed protonic and electronic conductors based on the double perovskite $\text{Ba}_{1-x}\text{Gd}_{0.8}\text{La}_{0.2+x}\text{Co}_2\text{O}_{6-\delta}$ have shown

promising performance.^[62] For NH_3 synthesis, studies have focused on identifying effective catalysts and two catalysts, Pd-Fe^[63] and VN-Fe,^[64] have shown improved ammonia production rates over traditional nickel-based catalysts.

2.2 | Plasma technologies

Gas discharge plasmas can be generated by supplying electrical energy to convert a gas into a plasma state. Neutral gas components are split into electrons and ions by ionization (among other chemical species). Seen from the outside, the gas remains neutral because it consists of equal numbers of negative and positive charges. A degree of ionization of 10^{-4} (1 in every 10 000 particles is ionized) is sufficient to imprint the typical collective behaviour of a plasma on the gas: plasma light emission, coupling to electric or magnetic fields, and extraordinary reactivity. To utilize the latter for chemical production, atmospheric pressure plasma processes are preferred with regard to energy efficiency and productivity. Avoiding vacuum and compression technologies enables the direct operation of plasmas with subsequent processes in the same pressure range.

In terms of their classification, atmospheric plasmas can be classified into “cold” (or non-thermal/non-equilibrium) and “hot” (or thermal/equilibrium) plasmas. Non-thermal or non-equilibrium plasmas are so called because the average kinetic energy (temperature) of the neutral gas molecules is the lowest and nearest to room temperature (also referred to as cold or warm), while electrons, the lightest particles in the plasma, have a higher temperature, often in the order of 10^4 Kelvin.^[65] Conversely, in thermal or equilibrium plasmas, the electron and the gas temperatures are more or less the same and are in the range of 4000–20 000 K. This is why they are also referred to as “hot plasmas”. A detailed description of plasma physics and technology can be found in the study of Fridman and Kennedy.^[66]

In the following sections, the “warm plasma” (a type of plasma in between the “cold” and “hot” plasmas, that is, the gas temperature ranges from 400–4000 K) and “hot plasma technologies”, which are mainly applied in CHEMampere, will be discussed more deeply. The terminology is also updated, with the term “low-temperature plasma” used to address the warm plasma technologies, which have gas temperatures in the typical range for thermocatalytic gas reactions (400–1000 K), and “high-temperature plasma” used for the hot plasma technologies, which have gas temperatures in the typical range for homogeneous radical gas reactions (>4000 K). An overview of the chemical reactions relevant for CHEMampere is given in Table 3.

TABLE 3 CHEMampere intermediates that can be produced directly from CO₂, N₂, O₂, and H₂O by low-temperature (LT) and/or high-temperature (HT) plasmas

Targeted chemical reactions	LT-plasma	HT-plasma ^a
$3\text{H}_2 + \text{N}_2 \rightleftharpoons 2\text{NH}_3$	X	X
$\text{N}_2 + \text{O}_2 \rightleftharpoons 2\text{NO}$	X	X
$3\text{O}_2 \rightleftharpoons 2\text{O}_3$	X	
$\text{CO}_2 + \text{H}_2\text{O} \rightleftharpoons \text{CO} + \text{H}_2 + \text{O}_2$	X	X
$\text{CO}_2 \rightleftharpoons \text{CO} + 1/2\text{O}_2$	X	X
$3\text{H}_2 + \text{CO}_2 \rightleftharpoons \text{CH}_3\text{OH} + \text{H}_2\text{O}$	X	

^aHT-plasmas indicated in this table are limited to those studied within CHEMampere (see Section 2.2.2).

2.2.1 | Low-temperature plasmas

Low-temperature plasmas can be created simply by applying an electric field between two electrodes (using either DC or AC). This causes the gas between the electrodes to partially break down into positive ions and (negatively charged) electrons. As the electrons are accelerated towards the positive electrode, they collide with the gas molecules, which can either ionize, excite, or dissociate the impacted molecules. Ionization processes generate new ions and electrons, and if they are emitted faster than they recombine, then the plasma becomes self-sustainable. Excited molecules will decay to the ground state (or another lower energy state) by emitting light, giving the plasma its characteristic colour (e.g., see Figure 10). Lastly, dissociation collisions lead to the formation of radical species, which react to form the products.

“Cold” plasmas, where the gas temperature is near room temperature, are, in general, appropriate for activating stable molecules such as O₂, N₂, and CO₂. However, electron density and discharge currents are too low (see Figure 6) for achieving productivities high enough for industrial production. Those cold plasmas can be applied to living tissues in cancer therapy by “producing” reactive oxygen and nitrogen species that tackle the tumour cells.^[67] This is where “warm” plasmas, which can be created by dielectric barrier discharges (DBDs) and DC-glow discharges, come into play, as they are both good at activating stable molecules and can provide good reactant conversion by allowing the translational temperature of the gas to be controlled to a certain degree.^[65] This is due to their higher electron density and lower average electron energy.

The power input is an important parameter, as it will dictate the type of plasma that will be generated. As can be seen in Figure 6, “warm” plasmas have a higher power input than “cold” plasmas thereby allowing the gas molecules to be heated to several hundred or even a thousand

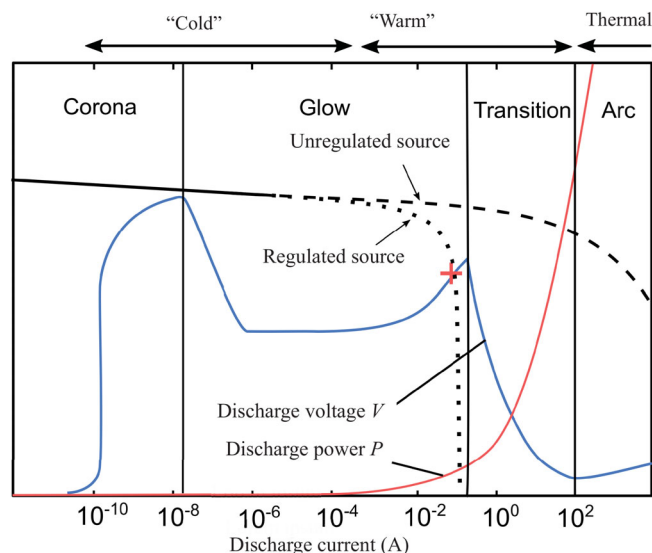
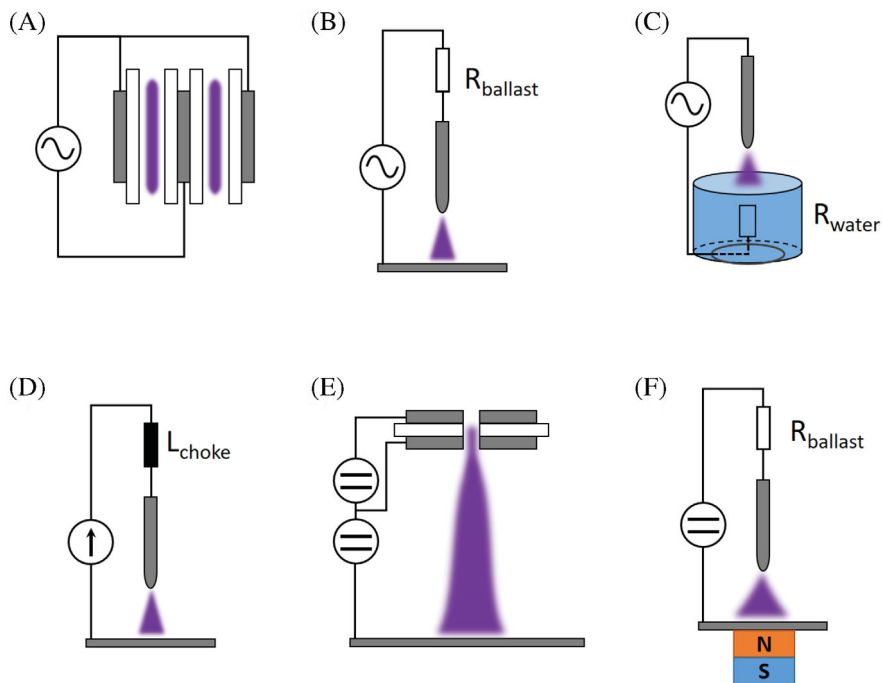


FIGURE 6 Exemplary direct current (DC) current characteristics of a typical plasma at atmospheric pressure. The discharge voltage is shown in blue and the plasma power in red. Different discharge regions are distinguished by vertical lines. The effect of using different types (regulated and unregulated) of voltage sources is depicted by the black lines. Dashed lines indicate the use of an unregulated source, while the dotted line shows the use of a regulated voltage source. The red cross indicates a stable point of operation

degrees Celsius. As the power input increases, so does the temperature of the gas and electrodes, until they get hot enough for thermal electron emission to occur. Thus, one challenge in creating “warm” plasmas is to prevent electrical breakdown and the transition of the plasma from a “warm” (non-thermal) plasma to a thermal plasma. The latter will be further detailed in Section 2.2.2.

Different approaches try to prevent “warm” plasmas from transitioning to a thermal plasma: One such strategy is to control the voltage using a regulated voltage source to limit the discharge current, which is marked in Figure 6 as a stable operation point. Another strategy is to place a dielectric material between the electrodes to limit the discharge current, thus creating a DBD. With such a barrier, an AC electric potential must be applied between the electrodes (with a frequency ranging from a few hertz to megahertz^[65]) to generate the DBD plasma (Figure 7A). However, the use of dielectrics is a major constraint for reactor design. This is why electronic components are also used (instead of a dielectric material) to limit the discharge current. A common laboratory setup for such plasmas consists of a pin- and a plate electrode, which is illustrated in Figure 7B–D,F for different power supplies. A ballast resistance can then be used to limit the discharge current (Figure 7B) and prevent the plasma from transitioning to a thermal plasma. This technique,

FIGURE 7 Schematic of different low-temperature plasma reactors. (A) Dielectric barrier discharge (DBD) reactor with two discharge gaps. (B) Pin to plate discharge with ballast resistor R_{ballast} . (C) Water is used as an anode, taking the additional role of a resistor R_{water} . (D) Smoothing inductor, L_{choke} , used in combination with a current source. (E) Hollow cathode discharge as a current-limiting electron emitter in a three-electrode setup. (F) Magnetic field in axial direction of pin to plate discharge



however, is only appropriate at the laboratory scale as a lot of energy is wasted in the resistor. A water electrode can be used instead, which handily combines cooling and electrical resistance (Figure 7C).^[68] This offers the additional possibility of involving water and dissolved chemicals like ammonia in chemical reactions. Discharge current limiting can also be achieved with power electronics and inductors, which is more efficient (Figure 7D). Three electrode geometries, where two electrodes serve as the current source and the third one accelerates the electrons, are employed for glow discharges as well (Figure 7E).^[69] An example of this is the hollow cathode discharge. Magnetic fields can be used to stabilize direct current (DC) discharges and increase their volume by changing the path of electrons in a DC glow discharge (Figure 7F).^[70] A further strategy is to generate very fast discharges (in the nanosecond range), which are referred to as nanosecond-pulse discharges.^[71]

Dielectric barrier discharges

DBDs have been in operation since the late 19th century, when they were used as a laboratory sources for ozone and nitrous oxides.^[72] When a high voltage alternating current is available, DBDs are easy to ignite and control, and have a simple design, facilitating catalyst implementation (see Section 2.2.3), which is why they gained popularity for the use in catalysis and endothermic processes. Since an alternator and a transformer are the only major components, efficient plasma sources are comparably easy to build, whereby the power can be tuned by altering frequency or voltage amplitude, and the specific energy can be tuned by regulating the gas flow.

DBDs can produce homogeneous glow discharges or streamer discharges depending on the electrode distance, gas mixture, pressure, and nature of the dielectrics.^[73] In a homogeneous discharge, power is evenly distributed within the volume of the plasma, while in a streamer discharge, the plasma forms thin channels between the opposing dielectrics where the totality of the current travels through, while the bulk of the gas remains unaffected. Glow discharges are harder to maintain, as they only appear in electrode setups with small gas gaps (in the millimetre range). Dielectric materials include polymers and ceramics, but silicate glass and alumina are the ones used most often.

DBDs can be built in a planar or tubular configuration. The planar configuration can be scaled up by stacking individual reactors. However, for large stacks, thermal issues arise, as good dielectrics are usually poor thermal conductors. At a discharge gap of just a few millimetres, the dielectrics are subject to a large heat flux from the gas. This is a problem not found in large volume discharges, for example, in microwave plasmas (see Section 2.2.2).^[74] This is also the reason why thermal processes are not expected to play a big role in DBDs, qualifying them as warm plasmas with an operation temperature in the range of hundreds of degrees Celsius.

DC-glow discharges

As discussed previously, a variety of plasma reactor designs is available to produce glow discharges, but they all require current control, which is why they have received less attention in plasma catalysis research.

However, DC glow discharges are also pursued within the CHEMampere initiative, because of their favourable characteristics for chemical processes, such as high-power density and easy thermal management. In terms of reactor designs already in use for CO₂ splitting (the most popular application), a tubular design using vortex flow was presented in 2019 by Trenchev et al.^[75] Just recently, Raja et al. used a vortex gas flow and ring electrodes to prevent arc formation.^[76] In a design, which will be further pursued for CHEMampere, collaborators of the initiative have presented a reactor using pin-discharge and an axial magnetic field,^[77] which does not utilize a vortex flow and can thus be operated at arbitrary gas flow rates.

The employed electrode geometry addresses another issue that is important when using glow discharges: gas flow and plasma discharges must match in shape. Gas is often conducted through a plasma while not utilizing the whole volume of the discharge, as illustrated in Figure 8A, which leads to a low energy efficiency. A similar problem arises in DBDs that operate in streamer mode as well as in DC glow discharge reactors that produce small discharge volumes: most of the gas does not pass through the discharge volume, leading to a low conversion, which is illustrated in Figure 8B. In contrast, in the pin-to-ring geometry with axial gas flow, all of the gas passes through the discharge volume, allowing the totality of the discharge to be utilized.

2.2.2 | High-temperature plasmas

High-temperature plasmas are thermal, or equilibrium, plasmas and can be generated either by high temperatures (4000–20 000 K) or high gas pressures. In both cases, collisions between electrons and the heavier species (e.g., molecules and atoms) become much more frequent. This increases the efficiency of the energy transfer from the electrons to the heavy species such that eventually an equilibrium is established between the temperatures of all particles in the plasma. Thermal plasmas can provide a high electron density, which is important for achieving

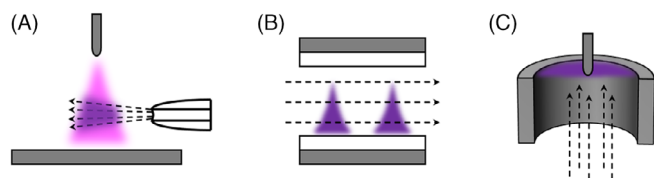


FIGURE 8 Different approaches for gas injection into the plasma; gas flow is indicated by arrows. (A) in pin-to-plate discharges, a large share of the plasma is often not used. (B) Conversely, gas can pass through the reactor unaffected when small discharges appear. (C) Pin-to-ring discharge as an example to balance both effects

high productivity. However, for chemical production, temperatures near the lower bound of the typical temperature range are, in most cases, sufficient to supply enough thermal energy to a gas or gas mixture to sustain or to operate chemical reactions. However, thermodynamics can cause restrictions on the conversion in the case of exothermic equilibrium reactions. For endothermic reactions (and products) such a thermodynamic limitation does not occur, and reaction rates can be massively enhanced through the high temperatures.

The technological use of a plasma discharge for chemical syntheses started around 1905 with the synthesis of nitrogen oxides for nitric acid production using the Birkeland–Eyde process.^[78,79] The production of higher hydrocarbons from methane began industrially before the Second World War, when the Hüls process for acetylene (ethine) synthesis was developed.^[80]

All of the early plasma processes were based on DC discharges. Due to the very cost-intensive electrical energy requirements, they were soon replaced by fossil materials and energy resources. In addition to the high costs, there was the issue of the short operating lifetime of the reactors due to the erosion of the electrodes. In order to increase the operation time of the electrodes, additional reactors with rotating gas flows have been designed, which cause the plasma arc to rotate, creating a moving starting spot for the discharge on the electrodes, thereby reducing the material's erosion rate. For the Hüls process as well as for the Birkeland–Eyde process, stationary magnetic fields have been used, whereby the resulting Lorentz forces force the plasma arcs to rotate. High frequencies (HF), from a few kilohertz to several megahertz, alternate the current flow. A rotating gas flow is also mandatory for HF technology. Arc technologies can therefore be divided into three groups: DC arc discharge with a rotating gas flow, DC arc discharge with a magnetic field, and HF arc discharge with a rotating gas flow.

Plasma arcs can be generated not only by applying a voltage between two electrodes but also by coupling alternating electromagnetic fields. The plasma state is generated by accelerating the electrons with the electric field. Meanwhile, the magnetic component is utilized through the so-called inductively coupled plasmas (ICP), meaning that a magnetic alternating field is generated in a discharge gap via a coil, which drives a current through the plasma. A high voltage spark is required to generate enough electrons and ions. Alternatively, the plasma can be ignited via the alternating electric field at low pressure and operated at atmospheric pressure afterwards. A typical excitation frequency is 13.56 MHz. At higher microwave frequencies, in the range of GHz, the electrical component of the alternating field is used. The field strength can be increased via resonator structures in such

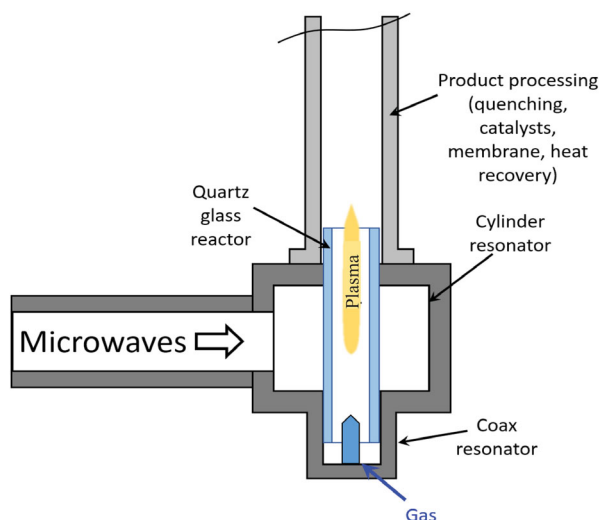


FIGURE 9 Scheme of the plasma torch for CHEMampere. It consists of a cylindrical resonator with a quartz glass tube reactor. A coaxial resonator is mounted under the cylindrical resonator for the ignition of a starting plasma. This starting plasma shifts into the central area of the cylinder resonator in order to form a free-standing, voluminous plasma. The plasma is stabilized by a rotating gas flow

a way that an independent ignition with subsequent operation takes place. A typical frequency is 2.45 GHz in the UHF band. This is a relatively inexpensive technology that is used, for example, in microwave ovens.

Microwave plasma torch

CHEMampere addresses high-temperature plasma technologies with microwave-powered plasmas. These can be used to generate electrodeless and easy-to-operate plasmas. The simple controllability of the available electricity from renewable energy sources, the scalability, and the adaptation to tubular reactors qualify them for plasma-chemical synthesis.

A novel arrangement of microwave resonators around a microwave-transparent reactor tube enables both the simple ignition of the plasma and the controllable continuous operation of different plasmas.^[81] Figure 9 shows the schematic view of the plasma torch used in CHEMampere. The microwave torch consists of a cylindrical resonator. In the simplest case, a quartz glass tube reactor is centrally arranged. A coaxial resonator is mounted under the cylindrical resonator. If the microwaves are coupled with the plasma torch via a waveguide, an excessive field arises at the tip of the coaxial resonator and causes the ignition of a “starting” plasma. This starting plasma shifts into the central area of the cylindrical resonator in order to form a free-standing, voluminous plasma. To stabilize the plasma, a rotating gas flow

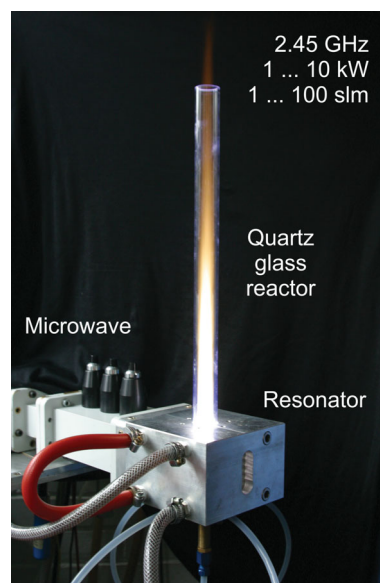


FIGURE 10 Picture of a microwave plasma torch designed for a microwave frequency of 2.45 GHz with an air plasma at 3 kW microwave power and an airflow of 30 standard litres per minute (slm). The rotating gas flow stabilizes the hot plasma inside the quartz glass tube above a length of 50 cm without damaging the quartz material

is generated in the coaxial resonator via tangential gas feeds.

Figure 10 shows the picture of a microwave plasma torch designed for a microwave frequency of 2.45 GHz with a power of 3 kW and an airflow of 30 standard litres per minute (slm). Spectroscopic measurements of the plasma with high-resolution spectrometers have shown a gas temperature of 3500 K. The rotating gas flow stabilizes the hot plasma inside the quartz glass tube above a height of 50 cm, without damaging the quartz material.^[74,81] Typical microwave powers are 1–10 kW with gas flows between 1–100 slm.

2.2.3 | Catalysts

Research on plasma catalysis is growing rapidly due to numerous applications such as volatile organic compound removal,^[82] ammonia synthesis,^[83–86] biogas conversion,^[87] methane coupling,^[88] cracking processes,^[89] and CO₂ conversion.^[65,90–94] When thinking in terms of plasma catalytic processes, it is important to mention that the concepts and types of thermal catalysis are not necessarily transferrable to plasma catalysis in a straightforward way. Some reasons for this are that the species that come into contact with the catalyst are different and may be activated and/or (partially) converted in the plasma phase.^[90,95,96] In addition, depending on the type of plasma and the

reactor configuration, a mutual influence of the catalyst on the plasma and vice versa may exist, for example, due to (di)electrical, discharge, local field, or photo effects, as well as divergent reaction conditions in terms of, for example, temperature and pressure.^[95,97] Therefore, catalysts need to be adapted to the plasma-based process and the chosen reactor configuration, which is currently a point of interest in research and a necessity in order to advance the field of plasma catalysis towards the selective production of chemicals in an energy-efficient way.

In general, a catalyst can be positioned with respect to the plasma in two distinct ways^[82]: (1) downstream of the plasma discharge (denoted as post-plasma catalysis—PPC—or two-stage configuration) or (2) directly in the plasma discharge zone (denoted as in-plasma catalysis—IPC—or one-stage configuration). Figure 11 shows the schematic of such configurations for the particular case of packed bed reactors, as they are the most used. However, other configurations,^[98] such as fluidized bed designs^[99] or catalytic-wall-reactors,^[88] do exist.

The PPC configuration, in which the catalyst is placed after the plasma discharge zone (i.e., the catalyst is not in contact with the plasma), is closest to the thermal catalytic processes but, as discussed above, is not necessarily equal since the feed gas composition and properties entering the catalytic zone depend on the plasma process. The catalyst comes, instead, into contact with the plasma-treated stream, which can consist of pre-converted molecules and/or activated long-living species, depending on the distance between the catalyst bed and the plasma discharge zone as well as on the stability of the activated species.^[90] When activated plasma species come into contact with the catalytic material, differences in adsorption and catalytic surface reactions can be expected, in comparison to classical thermal processes.^[95] Furthermore, the thermal aspects of the post-plasma catalytic reactions have to be taken into account. For example, when DBD reactors are used, the temperature of the gas phase in the PPC reaction zone is often relatively

mild and dependent on the plasma conditions (in the range of 100 to a few hundreds of degrees Celsius). Noteworthy is the fact that if the chemical factory adopts the ultra-efficiency concept, then reactions requiring higher temperatures can be performed, for example, by reusing the process/production site waste heat to achieve the temperature levels needed in the PPC reactor. Although the implementation of PPC might be feasible for some processes using low-temperature plasmas, it is particularly interesting to combine it with, for example, microwave and arc plasmas. In these cases, the heat produced in the plasma is much higher and can be recovered in the post-plasma catalytic reactor section to, for example, convert unreacted components or to perform a second-stage consecutive reaction, converting the plasma exhaust stream to products not accessible in the hot plasma zone. This way, different process units can be heat integrated, leading to an “all-electric” process and an enhancement of the efficiency of the entire process (see Section 4).

When working with IPC, the catalysts are placed directly in the plasma discharge zone. This configuration is particularly challenging for high-temperature plasmas, putting constraints on the compatibility of materials. Therefore, the IPC configuration is mainly employed using low-temperature plasmas, with the majority of studies involving packed-bed DBD reactors.^[65]

Contrary to what is seen with the PPC configuration, the IPC configuration is sensitive to the presence of packing materials in the plasma discharge zone due to the interaction between the packing material and the plasma and vice versa, which might or might not be catalytic in a classical (thermal) sense.^[90,95] This interaction can lead to physical^[90,97,98,100,101] or surface effects^[90,102–104] in the plasma. A few examples are changes in breakdown voltage, electron temperature, electric fields, discharge behaviour, number and displaced charge of streamers, surface charging, reductive capability, hot spot formation, photon fluxes, etc. In addition, sorption, quenching of species and/or catalytic effects can occur at the surface. Moreover, the material impact in IPC is strongly related

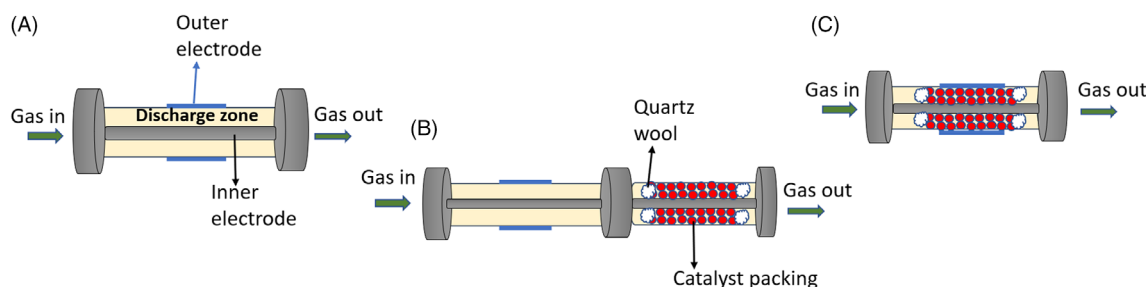


FIGURE 11 Different types of plasma configurations with a dielectric barrier discharge (DBD) reactor as an example: (A) non-catalytic, (B) post-plasma catalysis (PPC), and (C) in-plasma catalysis (IPC)

to the reactor design parameters^[105] (e.g., gap size), process conditions^[105] and materials properties (e.g., geometry, size/gap ratio^[106] and composition^[107,108]). Together, these effects can play different roles in enhancing or reducing the reaction performance in terms of conversion, selectivity, space-time yields, and energy efficiency. Lastly, it is worth pointing out that deactivation should also be considered differently in plasma catalysis, where the plasma can alter material properties (e.g., causing deactivation) or prevent/diminish deactivation processes such as coking or certain thermal deactivation mechanisms, creating new opportunities for application of the IPC configuration.^[88,96]

In addition to the several reviews and papers mentioned in the above discussion, the main current challenges and opportunities of plasma catalysis have been highlighted in the 2020 plasma catalysis roadmap, describing various aspects of research that cover the differences in plasma catalysis versus thermal catalysis, how to leverage thermal catalysis principles to plasma catalysis, catalyst selection methodologies with respect to the plasma/catalyst configuration, catalyst design, modelling, plasma-catalyst interactions, and the importance of in-situ diagnostic and experimental approaches.^[90]

2.3 | Ohmic resistance heating of reactors/catalysts

For endothermic chemical equilibria and endothermic irreversible reactions operated at temperatures above 600°C, most of the energy needed to drive the process is still supplied by the combustion of fossil fuels, such as methane. This significantly contributes to the direct CO₂ emissions of such processes, with those energy-related CO₂ emissions usually being much higher than the process-related ones since the chemical industry is an energy-intensive industry.^[8] In some cases, energy-related CO₂ emissions can be avoided by supplying the heat for thermocatalytic or thermochemical high-temperature reactions by direct electrical heating of the reactor/catalyst, which can additionally be considered to be safer and more flexible in comparison to burner and boiler technologies, since open flames or exhaust gases are nonexistent.^[109] Direct electrical heating can be carried out by resistive heating, microwave heating, and even with plasmas (see Section 2.2).

Within the chemical industry, a broad variety of electric heater designs are available, with the most typical designs based on resistive heating with, for example, rod-type heaters, heating plates, heating tapes, and heating mats. Regardless of the application and type of heat transfer, heating elements commonly consist of a spiral (metal) heat conductor, which is embedded in a

protective material to withstand stresses of chemical, thermal, and abrasive nature. However, such a configuration possesses two inherent drawbacks: the first is a relatively high thermal mass, which aggravates temperature controllability, and the second is a possibly inhomogeneous temperature distribution within the reactor/catalyst. Furthermore, semiconductors, for instance, silicon carbide (SiC) or molybdenum disilicide (MoSi₂), are also applied as heating elements, which present a good alternative, but possess limitations in processability and thus restrict design options.

The approach traced within CHEMampere involves developing electrical resistance heating materials, which act as a heat conductor and possess self-protecting properties at the same time, making the protective material dispensable. Another benefit can be found in the variety that can thereby be obtained. An illustrative example arises from the possibility of assembling electrically heated tubular reactors or tube bundles, which make fossil-powered pre-heaters obsolete. In the context of this feature article focussing on the direct conversion of air/water to CHEMampere intermediates, only CO₂ splitting into CO and O₂ fits into the underlying scheme. However, it should be kept in mind that the reverse water gas shift (RWGS) reaction is a further CHEMampere-related application of electrically heated reactors (see Table 4).

2.3.1 | Composite materials

Composites have emerged as a promising class of engineering materials offering new possibilities for modern technology and can be defined as materials consisting of two or more chemically and physically different phases, separated by a distinct boundary.^[110] The different components are merged to achieve a material with superior properties in comparison to the individual materials themselves.

In this context, the provision of process heat can occur by direct electric heating of conductive ceramic composites, whereby high thermal stability and good electrical conductivity represent key features of the demanded material. Cordierite ceramic is prominent for its advantageous

TABLE 4 CHEMampere intermediates that can be produced directly from CO₂, N₂, O₂, and H₂O by ohmic resistance heating of reactors/catalysts

Chemical reactions	ΔH° (kJ Mol ⁻¹) ^a
CO ₂ + H ₂ ⇌ CO + H ₂ O	+40.90
CO ₂ ⇌ CO + 1/2O ₂	+283.00

^aAt T = 298.15 K.

physical properties, for example, low thermal expansion and excellent thermal shock resistance, particularly for the application as a catalyst support. The insulating cordierite is combined with one or more conductive components for the formation of a conductive network and thus for the possibility of direct heating.

In the case of an insulator-conductor composite, the share of conductive filler within the insulating matrix material greatly influences the effective conductivity. At low filler concentrations, the electrically conductive particles are homogeneously distributed throughout the insulating matrix without or with hardly any interconnection.

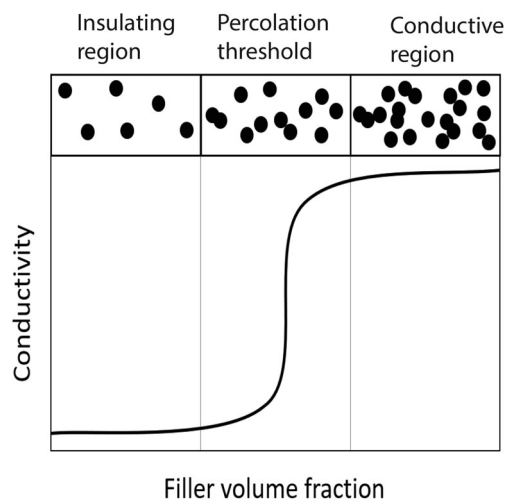


FIGURE 12 Schematic illustration of electrical conductivity for insulator-conductor composites as a function of the filler volume fraction

However, with an increasing volume fraction of conductive fillers, the formation of an interconnected network structure within the matrix material is possible. In the case of a binary system consisting of an insulator and a conductor, the electrical properties drastically change from insulating to conducting above the so-called critical percolation threshold, whereby the conductivity of the composite material is in the same range as that of the conductive filler, Figure 12.^[111,112]

The thermal stability and electrical conductivity of the developed ceramic composites are provided up to 1000°C under atmospheric conditions due to the formation of a protective layer on the composite material's surface, which, in turn, shields its core from further oxidation at elevated temperatures (Figure 13).^[113]

2.3.2 | Reactor designs

Concerning possible reactor designs for direct electric heating, all ceramic manufacturing techniques are applicable since the composite material's primary component is cordierite. In this context, the most relevant processes to be mentioned are compaction, extrusion, and additive manufacturing (see Figure 14). The compaction of ceramic powders provides a wide variety of sizes and shapes of the final product. The extrusion process produces objects with a fixed cross-sectional area and is thus suitable for manufacturing complex honeycomb structures or multitubular reactors. Additive manufacturing, particularly fused deposition moulding 3D printing of ceramic composites, is still only available for small volume

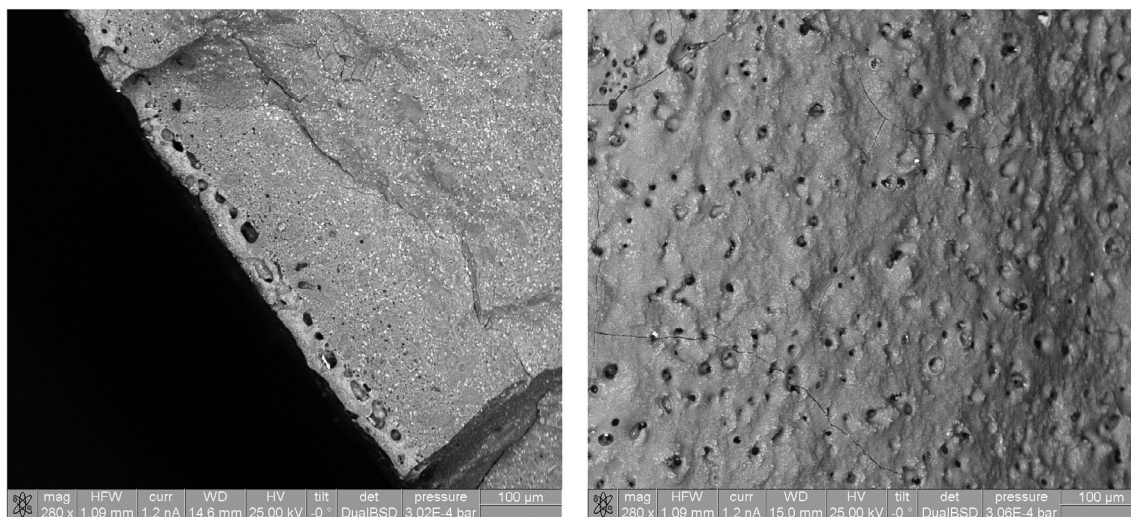


FIGURE 13 Scanning electron microscopy (SEM) images of the composite material (left) and its protective layer (right) due to high temperature exposure under atmospheric conditions (image is magnified 280×, the accelerating voltage was 25 kV, and the images were taken in high vacuum mode with a dual backscattered electron detector)

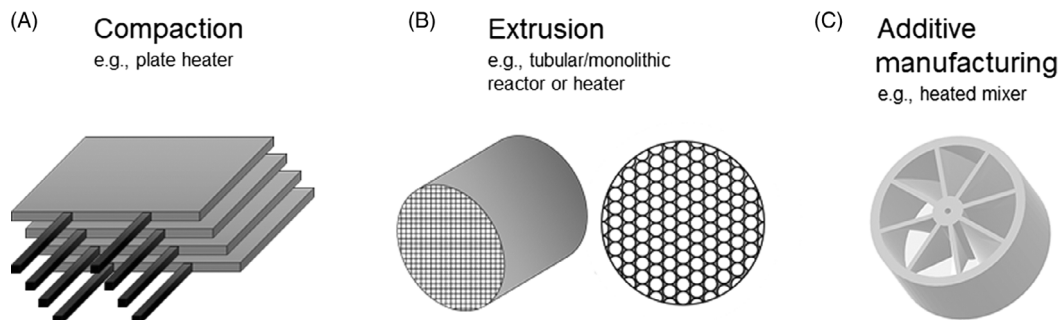


FIGURE 14 Types of ceramic processing methods: (A) compaction, (B) extrusion, and (C) additive manufacturing

production and is comparatively cost intensive. However, this manufacturing technique offers the possibility of creating complex structural elements without the need for preliminary tool costs, for instance, heated static mixers.

An interesting feature of ceramic composites, along with the aforementioned manufacturing methods, is the possibility of creating alternate segments of conductive composite material and insulating cordierite to more precisely influence the temperature distribution within/along the reactor. Another advantage is the possibility of coating the ceramic composite reactor with catalytically active components.

2.3.3 | Catalysts

One challenge with using ohmic resistance heating of reactors for heterogeneously catalyzed reactions is the availability, accessibility, and stability of a sufficient number of catalytically active sites. One solution to this problem is to coat a uniform catalytic layer on the conductive reactor walls. This can be done by directly coating the bulk catalyst or by first coating a support layer (washcoat) and then impregnating the active sites afterwards. Furthermore, the use of ceramic composite materials by themselves as bulk catalysts is currently being investigated, which necessitates incorporating the catalytically active sites into the composite. Another solution is to use the developed composite materials as (pre-) heating elements along with conventional reactors, for example, fixed- or fluidized bed reactors, in already existing and well-established process chains. The thermocatalytic CO_2 splitting into CO and O_2 , mentioned in the context of this article, is a highly endothermic reaction and thermodynamically unfavourable. Thus, either very high temperatures are needed (3000–3500 K) or one of the products must be withdrawn from the equilibrium to allow the reaction to proceed. This can be done at temperatures around 1000 K by a cyclic operation^[114] or using a membrane.^[65] Jin et al.^[115] used a SrCoFeZrO

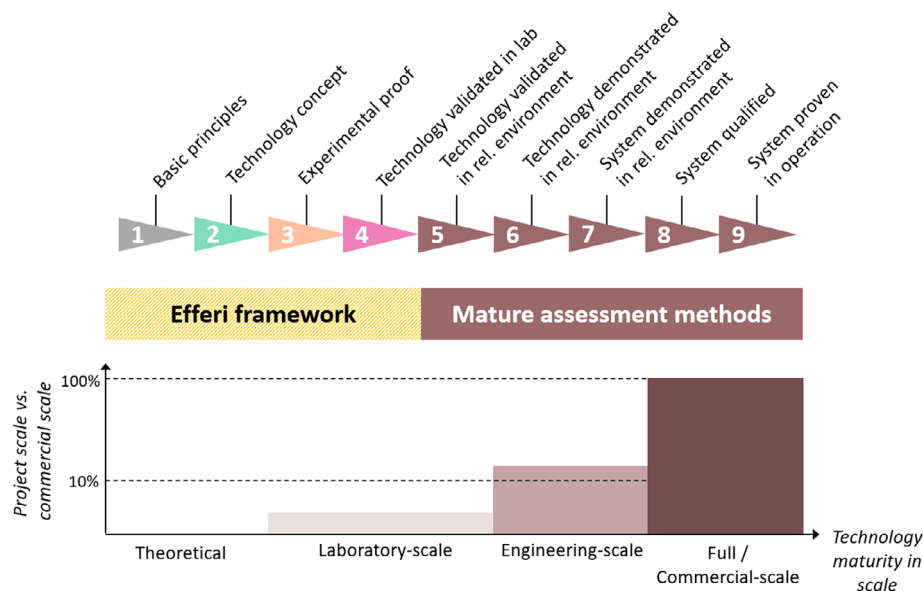
membrane and coupled the CO_2 reaction to the partial oxidation of methane to syngas to further increase the yield of CO . The best result obtained was a CO_2 conversion of nearly 15% at a temperature of 1120 K. So far, resistive heating with renewable electricity has not been applied in these processes. However, for the cyclic operation of CO_2 splitting, solar thermal power has been used as a renewable energy source.^[116]

While most strategies for splitting CO_2 into CO and O_2 either tend to veer towards high temperatures or the use of a membrane, a few studies have successfully shown the use of iron-based catalysts (Ni-ferrite, Co-ferrite, and Ni-doped iron oxide) for this application in reactors operated cyclically.^[114,117,118] In the context of RWGS, applied catalysts can be mainly classified into Cu-based (e.g., Cu-ZnO ^[119]), noble-metal-based (e.g., $\text{Pd/Al}_2\text{O}_3$, $\text{Pt/Al}_2\text{O}_3$, and Rh/SiO_2 ^[120,121]), reducible-oxide-based (e.g., CuO-NiO/SBA and $\text{CuO-CeO}_2/\text{SBA-15}$ ^[122]), and transition-metal-carbide-based catalysts (e.g., Mo_2C ^[123]).^[124]

3 | EVALUATION OF THE TECHNOLOGIES

To evaluate the maturity of the technologies presented so far in this text, the so-called TRLs are used. The most general and widely accepted scale across industries was first developed by NASA in 1974 and initially consisted of seven levels that were further expanded, in the 1990s, to the nine levels used nowadays.^[125] Recently, Zimmermann et al.^[126] developed a scale specific for the chemical industry (Figure 15).

Table 5 shows the evaluation of the technologies with regard to their TRL values for the conversion of CO_2 , N_2 , O_2 and H_2O to the intermediates NH_3 , NO_x , O_3 , H_2O_2 , H_2 , CO , and $\text{C}_x\text{H}_y\text{O}_z$. Thus, other reaction pathways such as CH_4 conversion towards ethylene or syngas (e.g., dry reforming) are not considered here, even though they can also contribute to a CO_2 -neutral production if green methane (biomethane, green synthetic natural gas) is

FIGURE 15 Technology readiness level scale developed by Zimmermann et al.^[126]

 TABLE 5 Estimated TRLs of the different technologies relevant to CHEMampere towards the direct production of the desired intermediates from CO₂, N₂, O₂, and H₂O as well as mixtures thereof

CHEMampere intermediates	LT-EL	O-SOE	H-SOE	LT-plasma	HT-plasma ^a	Ohmic resistance heating
NH ₃	1–2	1	2–3	2–3	1	n.p.
NO _x	1	n.p.	n.p.	2–3	4–5	n.p.
O ₃	n.p.	n.p.	n.p.	9	n.p.	n.p.
H ₂ O ₂	3–4	n.p.	n.p.	1–3 ^b	n.a.	n.p.
H ₂	7–9	6–8	3–4	1–3	n.a.	n.p.
CO	4–6	6–7	2–3	3	3–4	2–3
Syngas	2–3	6–7	2–3	2–3	1–3	2–3
HCOOH	3–4	n.p.	n.p.	n.a.	n.a.	n.p.
Methanol	2–3	n.p.	n.p.	1–3	1	n.p.
Ethanol	2–3	n.p.	n.p.	1–3	n.a.	n.p.
Ethylene	3–4	2–3 ^c	1–2 ^c	1–3 ^c	n.a.	n.p.
Propanol	2–3	n.p.	n.p.	n.a.	n.a.	n.p.

Note: n.p. means it is not possible or not reasonable to obtain the chemical with the corresponding technology. n.a. means it is not yet determined or not yet considered.

^aOnly microwave-sustained plasma torch processes are considered.

^bMay require post-plasma catalysis, for example, leading the gas from the plasma onto a catalyst bed.

^cIt should be noted that green methane can be converted to ethylene (and ethane) with both O-SOE and H-SOE, which is also relevant for a CO₂-neutral chemical value chain.^[127,128]

used. Furthermore, it is important to note that the TRL evaluation is done to the best of the authors' knowledge, based upon their own experience in CHEMampere projects such as EU projects as well as considering the state of the art.

From Table 5, it can be clearly seen that in the case of electrolysis technologies, water electrolysis, both at low temperature and at high temperature, has the highest

TRL values (6–9); in particular, alkaline electrolysis has already been fully commercialized for industrial applications but now requires further developments to account for the requirements of the energy transition. These developments are in the prototype and demonstration level aiming to reach the GW scale. A current European Green Deal Call addresses the demonstration of the 100 MW scale. The 1–10 MW scale is already

demonstrated by different companies such as Siemens (LT-EL), ITM Power (LT-EL), H-Tec Systems (LT-EL), or Sunfire (O-SOE). LT-CO₂EL to CO, ethylene and formic acid, and LT-O₂EL to H₂O₂ have reached TRL-levels of around 4. LT-CO₂EL to CO and formic acid have already been demonstrated by Siemens Energy and Dioxide Materials Inc. at high current densities of several 100 mA/cm² and faradaic efficiencies of at least 70% over more than 1000 h.^[29,129,130] Formic acid concentrations of up to 14 wt.% have been reached.^[129] For the LT-O₂EL towards H₂O₂ under acidic conditions, the highest concentrations reported in literature are around 1.2 wt.% at current densities of around 13 mA/cm² and faradaic efficiencies of nearly 40%.^[131] It must be noted that, in all cases, GDEs are used (see Section 2.1.1) to achieve the best results. Boosting low-temperature electrolysis technologies for CO₂ and O₂ reduction towards TRL 7 within 5 years should be doable, especially, when considering the knowledge gained in research and development of water electrolysis. For example, understanding the interplay of the electrode reactions with mass and heat transport, the transport activity nexus, is crucial to leverage the full potential of the technology for electrode reactions other than the hydrogen evolution reaction.^[132,133]

O-SOE, which is particularly attractive for a wider adoption of CO (and synthesis gas) production from CO₂ (and water), has been demonstrated both at the stack and system levels^[134,135] to outperform low-temperature electrolysis, in particular for the technical key performance indicators (faradaic efficiency, cell voltage, energy efficiency, and electric power consumption). H-SOE is at a lower TRL, but can still contribute to a CO₂-neutral value chain by non-oxidative dehydrogenation of short-chain hydrocarbons.^[54,136] Furthermore, H-SOE is the most promising approach for direct NH₃ production with high faradaic efficiencies of up to 70% at current densities of some mA/cm² when using H₂ oxidation as the proton source at the anode. However, when H₂O oxidation is performed at the anode to deliver the protons, faradaic efficiencies of 1% were not exceeded.^[137]

For ozone generation, DBD plasma technologies are already operated in potable and wastewater treatment, which corresponds to the highest TRL of 9. However, this technology has to be adapted to other CHEMampere-relevant chemical processes. For CO₂-splitting, Ozkan et al. validated the process in the laboratory (TRL 4) and achieved an energy efficiency of 22% at a conversion of 16%.^[138] Nonetheless, the prior knowledge and experience with the commercialization of the ozone generators can be expected to help drive other DBD plasma applications to higher TRL values. When using ballast resistors in the power supply instead of a dielectric, Trenchev et al. achieved 29% energy efficiency at 12% conversion

with a tubular design using vortex flow.^[75] Raja et al. also used a vortex gas flow, but ring electrodes to prevent arc formation, being rewarded with a high energy efficiency of 60% at conversions ranging from 2% to 3%.^[76] In a design that will be further pursued for CHEMampere, a reactor using pin-discharge and an axial magnetic field was presented, which achieved 27% energy efficiency at 17% conversion.^[77] It does not utilize a vortex flow and can thus be operated at arbitrary gas flow rates.

Catalysts implemented inside the low-temperature plasma must be adjusted to the reactor configuration and operational conditions of the plasma and vice-versa. This results in a complex interplay between catalysis and plasma that is not yet fully understood or controllable. Although the lack of understanding of this complex interplay is the reason for the current low TRL of 3, it also holds a high degree of freedom^[95,101,105] and potential to unlock alternative production processes that provide solutions for the current challenges in the transition to a more sustainable chemical production. Thus, current research efforts aiming to enhance understanding of plasma catalysis provide the potential for an increase to higher TRLs in the next few years.

In the case of the electrically heated reactors/catalysts, only the production of CO is possible by direct conversion of CO₂ with a TRL value of 2–3 (Table 5). However, the described concept of electrically heated reactors has been thoroughly investigated in the field of emission control for automotive applications. The technical maturity of conductive ceramic composites being used as catalyst support is between TRL 6 and 7, whereby the first prototypes are currently being developed and tested.^[113] Considering the knowledge gained during the research activities for the automotive sector, particularly concerning coating, contacting concepts, control, and regulation, it should be feasible to lift the initially stated TRL for the production of CO from 2–3 towards a TRL value of 5 within 3 years. Besides the direct conversion of CO₂ to CO, the technology of electrically heated reactors can also contribute to the conversion of CO₂ when reductants such as H₂ (RWGS reaction) and CH₄ (dry reforming) are used. Furthermore, the technology is also applicable to thermochemical or thermocatalytic cracking reactions such as steam reforming or deep catalytic cracking.

4 | EFFICIENCY OF CHEMICAL PRODUCTION WITH ELECTRICITY

Efficiency is an essential evaluation criterion both for a single process unit such as a reactor as well as for the whole process composed of several process units. In

general, the efficiency of a technical system is defined as the ratio of benefit to effort. The effort in our case is renewable electricity, which is utilized for activating CO_2 , N_2 , O_2 , and H_2O and converting them into the CHEMampere intermediates (see Figure 1). The benefit is the chemical itself, which makes the discussion of efficiencies more complicated. In the case of chemical energy storage where the energy content of the chemical is the benefit, the definition of the total energy efficiency $\eta_{el,LHV}$ can be written as follows^[139]:

$$\eta_{el,LHV} = \frac{\sum_P \dot{n}_P \cdot LHV_P}{P_{el} + \sum_R \dot{n}_R \cdot X_R \cdot LHV_R} \quad (1)$$

with \dot{n}_R and \dot{n}_P being the molar flow rates of the reactants (R) and products (P), X_R being the conversion of reactant, and P_{el} being the electrical power input. In the case of water electrolysis, the equation is reduced to:

$$\eta_{el,LHV} = \frac{\dot{n}_{\text{H}_2} \cdot LHV_{\text{H}_2}}{P_{el}} \quad (2)$$

However, in the case of the CHEMampere intermediates, it is the goal to further process such chemicals to their final products, rather than to use them as chemical energy storage media. Thus, “energy efficiency” as defined in Equation (1) has to be adjusted accordingly, that is, with the production rate of the intermediate as the benefit and the electrical power input as the effort:

$$\eta_{el,P} = \frac{\dot{n}_P}{P_{el}} \quad (3)$$

$\eta_{el,P}$ is not dimensionless because its value indicates the number of moles of product formed per kWh of electricity consumed. It is also sometimes referred to as energy yield, $Y_{el,P}$, which should be preferred because, strictly speaking, the term “energy efficiency” is incorrect from a thermodynamic point of view. The reciprocal of $Y_{el,P}$ is also called “specific energy consumption” or simply “energy cost”.

As is typical for every chemical process, the effort of producing a final product also depends on the material balances. Conversion of the reactants and selectivity towards the desired product determine the effort of reactant separation, reactant recirculation, and the purification of the product to meet the specification requirements. Thus, further electrical power input is needed, for example, for pumps and/or compressors, or heat input is needed for a distillation unit or for the absorbent regeneration in a scrubbing unit. However, this

affords the opportunity of heat recovery and utilization (heat integration), for example, by recovering the heat from the reactor unit, which can be either an electrolyzer, a plasma reactor, or an electrically heated catalytic reactor, and utilizing this heat in a distillation unit. So, the whole process must be balanced with regard to reactant and product components and energy, with electrical energy and heat being the main energy forms in the processes using the CHEMampere technologies described in the previous sections. The ultimate goal of the design of CHEMampere processes is to have renewable electricity as the sole energy input, which covers the energy demand of the whole process, leading to a so-called all-electric process.

To further increase the benefits of chemical production, we have to go beyond the process level, that is, not only considering material and energy balances but also following a holistic approach whereby emission, human/staff, and organization are considered. This leads to the concept of ultra-efficiency, which means reconciling both efficiency (using as few resources as possible) and effectiveness (producing as ecologically harmlessly as possible).^[122] Thus, to define what the target state of future manufacturing systems should be, the concept of an ultra-efficient factory can be used. Such factories should work in perfect symbiosis with their environment, addressing the five fields of action: material, energy, emissions, human/staff, and organization. The holistic and equal consideration of these fields of action from the process level up to the entire factory and its environment constitutes the uniqueness of the concept of the ultra-efficient factory, which represents an extended sustainability framework. By taking a holistic view of the defined five fields of action, conflicting goals, for example, between energy efficiency, emission reduction, and the yield of chemical processes, can be identified and thus resolved or even eliminated.^[23,24] When considering industrial energy systems, ultra-efficiency can contribute, for example, by integrating technologies to increase energy efficiency and flexibility as well as energy distribution and storage. The holistic consideration of the five fields of action ensures that environmental or social impacts are not shifted, for example, within the life cycle phases of a product, and actual improvements are achieved.

5 | CONCLUSIONS

Electricity-based CCU technologies producing green chemicals directly from CO_2 , N_2 , O_2 , and H_2O , without a detour via green hydrogen, are needed because the demand for green hydrogen will rise dramatically due to

the decarbonization of the energy sector, which will cause a conflict of use between chemistry and the energy sector similar to crude oil nowadays. An electrochemical refinery (e-Refinery) based upon green hydrogen from H₂O electrolysis is certainly a possibility to produce green methanol (methanol economy), green ammonia, or green hydrogen peroxide from CO₂, N₂, and O₂ with capacities of several 100 000 tonnes up to a million tonnes. However, this needs tremendous capacities of renewable-energy power plants in the range of hundreds of Gigawatts. On the other hand, there are several routes for electricity-driven chemical processes to produce chemicals without the detour via green hydrogen, such as direct production of hydrocarbons, H₂O₂, HNO₃, etc. It is the belief of collaborators of the CHEMampere consortium that even commodities such as methanol can be produced on demand in a decentralized manner in the amounts needed for the respective production process. Since renewable electricity is mainly produced and distributed in a decentralized manner, it makes sense to couple chemical production to these sources, which in turn also implies that chemical production has to be done in a decentralized and distributed manner. For example, the Fraunhofer ISE institute has estimated that, in Germany, there is the potential for building envelopes to provide up to 800 GW of peak power, and even agrivoltaics has the potential to provide up to 1.7 Terawatts of peak power.^[140]

As a consequence of such a decentralized CO₂-neutral chemical factory of the future relying on renewable electricity to drive chemical reactions, new factory concepts are needed that follow a holistic approach equally considering the following fields: material, energy, emissions, human/staff, and organization. The so-called ultra-efficiency concept provides such a holistic approach, for example, by integrating technologies to increase efficiency and flexibility as well as energy distribution and storage. The energy efficiency of a chemical process should not be evaluated by considering the heating value of the chemical product as its benefit but rather by considering the exergetic efficiency of the whole electricity-based process, meaning that heat integration, recovery, and storage are also considered. Doing so allows exergetic efficiencies above 80% to be reached.

Evaluation of the electricity-driven core reactor technologies of CHEMampere has shown that within the next 5–10 years (so until around 2030), the following intermediates might be produced on a t/h-scale directly from CO₂, air, water, and renewable electricity:

- NH₃ by reductive N₂ activation through high-temperature electrolysis with H-SOC.
- NO_x (HNO₃, nitroaromatics, etc.) by oxidative N₂ activation with high-temperature microwave plasma reactors.
- O₃ by O₂ conversion with a DBD plasma (already applied in potable and wastewater treatment with ozone production capacities of over 250 kg/h^[141]).
- H₂O₂ by O₂ conversion through low-temperature electrolysis.
- CO (and syngas) by CO₂ (and water) conversion through high-temperature (co-)electrolysis with oxygen ion conducting solid oxide electrolysis cells (O-SOC).
- C_xH_yO_z (e.g., formic acid, ethylene, and alcohols) by CO₂/H₂O conversion through low-temperature electrolysis.

It has to be noted that there are several more industrially promising chemical routes when utilizing green H₂ and methane for activating CO₂ with plasma or thermocatalytically with resistive heating.

ACKNOWLEDGEMENTS

The authors of this manuscript wish to acknowledge the University of Stuttgart for their support of the CHEMampere initiative. V. M. acknowledges the Research Foundation—Flanders (FWO) for grant number: K801621N and for their support to the PlasmaCatDESIGN project (FWO-SBO grant number: S001619N). A. S. and L. W. acknowledge the Ministry of the Environment, Climate Protection and the Energy Sector Baden-Württemberg for funding the research project “Ultra-efficiency Factory” (grant number: BWDU20101); S. R. acknowledges the German BMWi (Bundesministerium für Wirtschaft und Energie—Federal Ministry for Economic Affairs and Energy) for financial support towards the PlasmaFuel project (grant number: 03EIV161A). R. C. and K. A. F. acknowledge the German Federal Ministry of Education and Research (BMBF) for the funding of the Kopernikus P2X II (grant number: 03SFKE20-2), ARCADE (grant number: 03SF0580A), and DAICHI (Grant number: 01DR18002) projects. E. K., A. L., and C. L. also acknowledge the German BMWi for financial support (grants numbers: 03ET1379A and 03ET1642D), as well as the German BMBF for financial support (CO₂-WIN program, grant number: 033RC023E), and the European Union for the funding from the Horizon 2020 research and innovation programme under grant agreement number: 763911 (eForFuel). A. S. acknowledges the project consortium of the P2X project of the German Kopernikus initiative and the project partners of the Kopernikus satellite project PiCK for excellent cooperation. Open Access funding enabled and organized by Projekt DEAL.

AUTHOR CONTRIBUTIONS

Elias Klemm: Conceptualization; project administration; supervision; writing – original draft. **Carlos M. S.**

Lobo: Writing – original draft; writing – review and editing. **Armin Löwe:** Investigation; writing – original draft. **Verena Schallhart:** Investigation; writing – original draft. **Stephan Renninger:** Investigation; writing – original draft. **Lara Waltersmann:** Investigation; writing – original draft. **Rémi Costa:** Writing – original draft. **Andreas Schulz:** Investigation; writing – original draft. **Ralph-Uwe Dietrich:** Writing – original draft. **Lukas Möltner:** Investigation; writing – original draft. **Vera Meynen:** Writing – original draft; writing – review and editing. **Alexander Sauer:** Investigation; writing – original draft. **K. Andreas Friedrich:** Investigation; writing – original draft.

PEER REVIEW

The peer review history for this article is available at <https://publons.com/publon/10.1002/cjce.24397>.

DATA AVAILABILITY STATEMENT

Data sharing is not applicable to this article as no new data were created or analyzed in this study.

ORCID

Elias Klemm  <https://orcid.org/0000-0003-3235-5511>

Carlos M. S. Lobo  <https://orcid.org/0000-0002-7727-008X>

Armin Löwe  <https://orcid.org/0000-0001-5149-781X>

Verena Schallhart  <https://orcid.org/0000-0001-7942-2545>

Lara Waltersmann  <https://orcid.org/0000-0003-4606-4985>

Rémi Costa  <https://orcid.org/0000-0002-3534-1935>

Ralph-Uwe Dietrich  <https://orcid.org/0000-0001-9770-4810>

Lukas Möltner  <https://orcid.org/0000-0002-4569-3045>

Vera Meynen  <https://orcid.org/0000-0002-9867-6986>

Alexander Sauer  <https://orcid.org/0000-0003-3822-1514>

K. Andreas Friedrich  <https://orcid.org/0000-0002-2968-5029>

NOMENCLATURE

AEM	anion exchange membrane
BPM	bipolar membrane
CAPEX	capital expenditure
CCU	carbon capture and utilization
CEM	cation exchange membrane
CGO	gadolinium doped ceria
CSC	cathode supported cell
DBD	dielectric barrier discharge
ESC	electrolyte supported cell
FDM	fused deposition moulding
GDE	gas diffusion electrode
GW	gigawatt

HER	hydrogen evolution reaction
HF	high frequency
H-SOC	proton conducting solid oxide cell
ICP	inductively coupled plasma
IPC	in-plasma catalysis
IPCC	intergovernmental panel on climate change
LHV	lower heating value
LT-CO ₂ EL	low-temperature CO ₂ electrolysis
LT-N ₂ EL	low-temperature N ₂ electrolysis
LT-O ₂ EL	low-temperature O ₂ electrolysis
LT-WEL	low-temperature water electrolysis
MEA	membrane electrode assembly
MW	megawatt
OER	oxygen evolution reaction
O-SOC	oxygen ion conducting solid oxide cell
PCC	proton conducting ceramic
PEMWEL	proton exchange membrane water electrolysis
PPC	post-plasma catalysis
RWGS	reverse water gas shift reaction
SBA	a type of mesoporous silica
SEM	scanning electron microscopy
SOC	solid oxide cell
SOE	solid oxide electrolysis
SSRS	solid-state reactive sintering
TRL	technology readiness level
YSZ	yttria-stabilized zirconia

ENDNOTES

- Ultra-efficiency is defined as the multiplication result of efficiency and effectivity.
- <https://www.chemampere.com>.
- Synthesis gas is a mixture of CO and H₂.
- Anolyte/catholyte is the electrolyte in the anode/cathode chamber, respectively.

REFERENCES

- V. Masson-Delmotte, P. Zhai, H. O. Pürtner, D. Roberts, J. Skea, P. R. Shukla, A. Pirani, W. Moufouma-Okia, C. Péan, R. Pidcock, S. Connors, J. B. R. Matthews, Y. Chen, X. Zhou, M. I. Gomis, E. Lonnoy, T. Maycock, M. Tignor, T. Waterfield, Eds., *Global Warming of 1.5°C. An IPCC Special Report on the Impacts of Global Warming of 1.5°C Above Pre-Industrial Levels and Related Global Greenhouse Gas Emission Pathways, in the Context of Strengthening the Global Response to the Threat of Climate Change, Sustainable Development, and Efforts to Eradicate Poverty*, IPCC, Geneva, Switzerland **2018**.
- United Nations Department of Economic and Social Affairs, Population Division, *World Population Prospects 2019: Highlights*, **2019**, https://population.un.org/wpp/Publications/Files/WPP2019_Highlights.pdf (accessed: October 2021).
- K. L. Ricke, R. J. Millar, D. G. MacMartin, *Sci. Rep.* **2017**, *7*, 14743. <https://doi.org/10.1038/s41598-017-14503-9>.

- [4] United Nations Climate Ambition Alliance: Net Zero 2050, http://climateinitiativesplatform.org/index.php/Climate_Ambition_Alliance:_Net_Zero_2050 (accessed: March 2021).
- [5] United Nations Report of the Conference of the Parties on its Twenty-Fifth Session, Held in Madrid from 2 to 15 December 2019 (FCCC/CP/2019/13/Add.1) Madrid, 2019, https://unfccc.int/sites/default/files/resource/cp2019_13a01_adv.pdf (accessed: June 2021).
- [6] P. Friedlingstein, M. O'Sullivan, M. W. Jones, R. M. Andrew, J. Hauck, A. Olsen, G. P. Peters, W. Peters, J. Pongratz, S. Sitch, C. Le Quéré, J. G. Canadell, P. Ciais, R. B. Jackson, S. Alin, L. E. O. C. Aragão, A. Arneeth, V. Arora, N. R. Bates, M. Becker, A. Benoit-Cattin, H. C. Bittig, L. Bopp, S. Bultan, N. Chandra, F. Chevallier, L. P. Chini, W. Evans, L. Florentie, P. M. Forster, T. Gasser, M. Gehlen, D. Gilfillan, T. Gkitzalis, L. Gregor, N. Gruber, I. Harris, K. Hartung, V. Haverd, R. A. Houghton, T. Ilyina, A. K. Jain, E. Joetjzer, K. Kadono, E. Kato, V. Kitidis, J. I. Korsbakken, P. Landschützer, N. Lefèvre, A. Lenton, S. Lienert, Z. Liu, D. Lombardozzi, G. Marland, N. Metzl, D. R. Munro, J. E. M. S. Nabel, S.-I. Nakaoka, Y. Niwa, K. O'Brien, T. Ono, P. I. Palmer, D. Pierrot, B. Poulter, L. Resplandy, E. Robertson, C. Rödenbeck, J. Schwinger, R. Séférian, I. Skjelvan, A. J. P. Smith, A. J. Sutton, T. Tanhua, P. P. Tans, H. Tian, B. Tilbrook, G. van der Werf, N. Vuichard, A. P. Walker, R. Wannikhof, A. J. Watson, D. Willis, A. J. Wiltshire, W. Yuan, X. Yue, S. Zaehle, *Earth Syst. Sci. Data* **2020**, *12*(4), 3269.
- [7] J.-B. Vennekötter, T. Scheuermann, R. Sengpiel, M. Wessling, *J. CO₂ Util.* **2019**, *32*, 202.
- [8] IEA, *Chemicals*, IEA, Paris, France **2020**. <https://www.iea.org/reports/chemicals>.
- [9] R. Geres, A. Kohn, S. Lenz, F. Ausfelder, A. M. Bazzanella, A. Möller, *Working towards a Greenhouse Gas Neutral Chemical Industry in Germany*, FutureCamp Climate GmbH, München, Germany **2019**.
- [10] Global Carbon Atlas, <http://www.globalcarbonatlas.org/en/CO2-emissions> (accessed: August 2021).
- [11] Environment and Climate Change Canada. Greenhouse Gas Sources and Sinks: Executive Summary 2021, <https://www.canada.ca/en/environment-climate-change/services/climate-change/greenhouse-gas-emissions/sources-sinks-executive-summary-2021.html#es-3>. Published 2021 (accessed: December 2021).
- [12] M. Fasihi, O. Efimova, C. Breyer, *J. Clean. Prod.* **2019**, *224*, 957.
- [13] C. Breyer, M. Fasihi, A. Aghahosseini, *Mitig. Adapt. Strat. Gl.* **2020**, *25*(1), 43.
- [14] M. Sharifzadeh, L. Wang, N. Shah, *Renew. Sust. Energ. Rev.* **2015**, *47*, 151.
- [15] M. Jacoby, *Chem. Eng. News* **2020**, *98*(45), 26.
- [16] A. H. Tullo, *Chem. Eng. News* **2021**, *99*(9), 20.
- [17] L. Krietsch, *Chem. Eng. News* **2019**, *97*(24), 18.
- [18] Grand View Research Plastic Market Size, Share & Trends Analysis Report By Product (PE, PP, PU, PVC, PET, Polystyrene, ABS, PBT, PPO, Epoxy Polymers, LCP, PC, Polyamide), By Application, By End-Use, By Region, And Segment Forecasts, 2021–2028.; (978-1-68038-232-7) 2021, <https://www.grandviewresearch.com/industry-analysis/global-plastics-market> (accessed: June 2021).
- [19] Grand View Research Dyes & Pigments Market Size, Share & Trends Analysis Report By Product (Pigments, Dyes), By Application (Paints & Coatings, Printing Inks, Textiles), By Region (APAC, Europe), And Segment Forecasts, 2021–2028 (GVR-1-68038-545-8). 2021, <https://www.grandviewresearch.com/industry-analysis/dyes-and-pigments-market> (accessed: June 2021).
- [20] Polaris Market Research Laundry Detergent Market Share, Size, Trends, Industry Analysis Report, By Product (Powder, Liquid, Fabric Softeners, Detergent Tablets, Washing Pods, Natural/Eco-Friendly Detergents), By Application (Household, Industrial/Institutional); By Regions; Segm. (PM1489) 2021, <https://www.polarismarketresearch.com/industry-analysis/laundry-detergent-market> (accessed: June 2021).
- [21] Global Adhesives Market Size By Technology (Water Based, Solvent Based, Hot Melt, Reactive & Other), By Product (Acrylic, PVA, Polyurethanes, Styrenic Block, Epoxy And EVA), By Application (Pressure Sensitive Applications, Packaging, Construction, Furnitu. (GMI372). 2021, <https://www.gminsights.com/industry-analysis/adhesives-and-sealants-market-report> (accessed: June 2021).
- [22] T. Kuhlmann, A. Sauer, *Adv. Mater. Res.* **2016**, *1140*, 481.
- [23] L. Waltersmann, S. Kiemel, Y. Amann, A. Sauer, *Proc. CIRP.* **2019**, *81*, 1142.
- [24] L. Waltersmann, S. Kiemel, I. Bogdanov, J. Lettgen, R. Miehe, A. Sauer, J. Mandel, *Procedia Manufacturing* **2019**, *39*, 685.
- [25] M. Schutzbach, J. Full, S. Kiemel, L. Waltersmann, L. Sielaff, R. Miehe, A. Sauer, *Chem.-Ing.-Tech.* **2021**, *93*(11), 1.
- [26] K. van Kranenburg, E. Schols, H. Gelevert, R. de Kler, Y. van Delft, M. Weeda, *Empowering the Chemical Industry [White Paper]*, **2016**. https://www.tno.nl/media/7514/voltachem_electrification_whitepaper_2016.pdf (accessed: October 2021).
- [27] S. Takkellapati, T. Li, M. A. Gonzalez, *Clean. Technol. Envir.* **2018**, *20*(7), 1615.
- [28] N. J. Claassens, C. A. R. Cotton, D. Kopljar, A. Bar-Even, *Nature Catalysis* **2019**, *2*(5), 437.
- [29] T. Haas, R. Krause, R. Weber, M. Demler, G. Schmid, *Nature Catalysis* **2018**, *1*(1), 32.
- [30] G. A. Olah, A. Goepfert, G. K. S. Prakash, *Beyond Oil and Gas: The Methanol Economy*, 2nd ed., Wiley-VCH, Weinheim, Germany **2009**. <https://doi.org/10.1002/9783527627806>.
- [31] O. Z. Sharaf, M. F. Orhan, *Renew. Sust. Energ. Rev.* **2014**, *32*, 810.
- [32] R. Pinsky, P. Sabharwall, J. Hartvigsen, J. O'Brien, *Prog. Nucl. Energ.* **2020**, *123*, 103317. <https://doi.org/10.1016/j.pnucene.2020.103317>.
- [33] A. Löwe, C. Rieg, T. Hierlemann, N. Salas, D. Kopljar, N. Wagner, E. Klemm, *ChemElectroChem* **2019**, *6*(17), 4497.
- [34] T. Burdyny, W. A. Smith, *Energ. Environ. Sci.* **2019**, *12*(5), 1442.
- [35] J. Zhang, W. Luo, A. Züttel, *J. Catal.* **2020**, *385*, 140.
- [36] H. Li, C. Oloman, *J. Appl. Electrochem.* **2007**, *37*(10), 1107.
- [37] D. A. Salvatore, C. M. Gabardo, A. Reyes, C. P. O'Brien, S. Holdcroft, P. Pintauro, B. Bahar, M. Hickner, C. Bae, D. Sinton, E. H. Sargent, C. P. Berlinguette, *Nature Energy* **2021**, *6*(4), 339.
- [38] M. E. Leonard, L. E. Clarke, A. Forner-Cuenca, S. M. Brown, F. R. Brushett, *ChemSusChem* **2020**, *13*(2), 400.
- [39] J. J. Kaczur, H. Yang, Z. Liu, S. D. Sajjad, R. I. Masel, *Front. Chem.* **2018**, *6*, 263.
- [40] Y. Chen, J. A. Wrubel, E. Klein, S. Kabir, W. A. Smith, K. C. Neyerlin, T. G. Deutsch, *ACS Applied Polymer Materials* **2020**, *2*(11), 4559.

- [41] D. M. A. Dueñas, M. Riedel, M. Riegraf, R. Costa, K. A. Friedrich, *Chem.-Ing.-Tech.* **2020**, 92(1–2), 45.
- [42] M. Riegraf, A. Zekri, M. Knipper, R. Costa, G. Schiller, K. A. Friedrich, *J. Power Sources* **2018**, 380, 26.
- [43] M. Riegraf, M. P. Hoerlein, R. Costa, G. Schiller, K. A. Friedrich, *ACS Catal.* **2017**, 7(11), 7760.
- [44] S. K. Schubert, M. Kusnezoff, A. Michaelis, S. I. I. Bredikhin, *J. Power Sources* **2012**, 217, 364.
- [45] J. Mermelstein, M. Millan, N. Brandon, *J. Power Sources* **2010**, 195(6), 1657.
- [46] B. Iwanschitz, J. Sfeir, A. Mai, M. Schütze, *J. Electrochem. Soc.* **2010**, 157(2), B269.
- [47] M. Riegraf, R. Costa, G. Schiller, K. A. Friedrich, S. Dierickx, A. Weber, *J. Electrochem. Soc.* **2019**, 166(13), F865.
- [48] S. R. Foit, I. C. Vinke, L. de Haart, R. A. Eichel, *Angew Chem. Int. Edit.* **2017**, 56(20), 5402.
- [49] M. Riedel, M. P. Heddrich, K. A. Friedrich, *J. Electrochem. Soc.* **2020**, 167(2), 24504. <https://doi.org/10.1149/1945-7111/ab6820>.
- [50] M. Riedel, M. P. Heddrich, A. Ansar, Q. Fang, L. Blum, K. A. Friedrich, *J. Power Sources* **2020**, 475, 228682. <https://doi.org/10.1016/j.jpowsour.2020.228682>.
- [51] M. Riedel, M. P. Heddrich, K. A. Friedrich, *Fuel Cells* **2020**, 20(5), 592.
- [52] H. Iwahara, T. Esaka, H. Uchida, N. Maeda, *Solid State Ionics* **1981**, 3–4, 359.
- [53] B. L. Kee, D. Curran, H. Zhu, R. J. Braun, S. C. DeCaluwe, R. J. Kee, S. Ricote, *Membranes* **2019**, 9(7), 77.
- [54] C. Duan, J. Huang, N. Sullivan, R. O’Hayre, *Appl. Phys. Rev.* **2020**, 7, 11314. <https://doi.org/10.1063/1.5135319>.
- [55] X. Li, X. Ren, X. Liu, J. Zhao, X. Sun, Y. Zhang, X. Kuang, T. Yan, Q. Wei, D. Wu, *J. Mater. Chem. A* **2019**, 7(6), 2524.
- [56] S. C. Perry, D. Pangotra, L. Vieira, L.-I. Csepei, V. Sieber, L. Wang, C. Ponce de León, F. C. Walsh, *Nature Reviews Chemistry* **2019**, 3(7), 442.
- [57] J. Chi, H. Yu, *Chinese J. Catal.* **2018**, 39(3), 390.
- [58] C. G. Vayenas, R. E. White, M. E. Gamboa-Aldeco, Eds., *Modern Aspects of Electrochemistry*, Springer, New York **2008**.
- [59] M. B. Mogensen, A. Hauch, X. Sun, M. Chen, Y. Tao, S. D. Ebbesen, K. V. Hansen, P. V. Hendriksen, *Fuel Cells* **2017**, 17(4), 434.
- [60] M. P. Hoerlein, M. Matthias Riegraf, R. Costa, G. Schiller, K. A. Friedrich, *Electrochim. Acta* **2018**, 276, 162.
- [61] A. Hauch, S. D. Ebbesen, S. H. Jensen, M. Mogensen, *J. Electrochem. Soc.* **2008**, 155(11), B1184.
- [62] E. Vøllestad, R. Strandbakke, M. Tarach, D. Catalán-Martínez, M.-L. Fontaine, D. Beeff, D. R. Clark, T. Serra, J. M. Norby, *Nat. Mater.* **2019**, 18, 752.
- [63] S. Klinsrisuk, J. T. S. Irvine, *Catal. Today* **2017**, 286, 41.
- [64] V. Kyriakou, I. Garagounis, A. Vourros, E. Vasileiou, M. Stoukides, *Joule* **2020**, 4(1), 142.
- [65] R. Snoeckx, A. Bogaerts, *Chem. Soc. Rev.* **2017**, 46, 5805.
- [66] A. A. Fridman, L. A. Kennedy, *Plasma Physics and Engineering*, Taylor & Francis Books Inc., New York **2004**.
- [67] X. Dai, K. Bazaka, E. W. Thompson, K. Ostrikov, *Cancers* **2020**, 12(11), 3360. <https://doi.org/10.3390/cancers12113360>.
- [68] P. Bruggeman, J. Liu, J. Degroote, M. G. Kong, J. Vierendeels, C. Leys, *J. Phys. D Appl. Phys.* **2008**, 41(21), 215201. <https://doi.org/10.1088/0022-3727/41/21/215201>.
- [69] R. H. Stark, K. H. Schoenbach, *Appl. Phys. Lett.* **1999**, 74(25), 3770.
- [70] Y. S. Wang, W. D. Ding, J. Q. Yan, Y. N. Wang, *AIP Adv.* **2017**, 7(9), 95209. <https://doi.org/10.1063/1.4987031>.
- [71] D. Wang, T. Namihira, *Plasma Sources Sci. T.* **2020**, 29(2), 23001. <https://doi.org/10.1088/1361-6595/ab5bf6>.
- [72] U. Kogelschatz, *Plasma Chem. Plasma P.* **2003**, 23(1), 1.
- [73] Z. Fang, J. Lin, X. Xie, Y. Qiu, E. Kuffel, *J. Phys. D Appl. Phys.* **2009**, 42(8), 85203. <https://doi.org/10.1088/0022-3727/42/8/085203>.
- [74] A. Schulz, P. Büchele, E. Ramisch, O. Janzen, F. Jimenez, C. Kamm, J. Kopecki, M. Leins, S. Merli, H. Petto, F. R. Mendez, J. Schneider, U. Schumacher, M. Walker, U. Stroth, *Contrib. Plasm. Phys.* **2012**, 52(7), 607.
- [75] G. Trenchev, A. Nikiforov, W. Wang, S. Kolev, A. Bogaerts, *Chem. Eng. J.* **2019**, 362, 830.
- [76] B. Raja, R. Sarathi, R. Vinu, *Energy Technol.-Ger.* **2020**, 8(12), 2000535. <https://doi.org/10.1002/ente.202000535>.
- [77] S. Renninger, M. Lambarth, K. P. Birke, *J. CO2 Util.* **2020**, 42, 101322. <https://doi.org/10.1016/j.jcou.2020.101322>.
- [78] I. Remsen, *American Chemical Journal*, **1906**, XXXV, 358.
- [79] M. Alger, *Sci. Am.* **1906**, 95(14), 250.
- [80] H. Gladisch, *Chem.-Ing.-Tech.* **1969**, 41(4), 204.
- [81] M. Leins, M. Walker, A. Schulz, U. Schumacher, U. Stroth, *Contrib. Plasm. Phys.* **2012**, 52(7), 615.
- [82] J. C. Whitehead, *Pure Appl. Chem.* **2010**, 82(6), 1329.
- [83] P. Peng, P. Chen, C. Schiappacasse, N. Zhou, E. Anderson, D. Chen, J. Liu, Y. Cheng, R. Hatzenbeller, M. Addy, Y. Zhang, Y. Liu, R. Ruan, *J. Clean. Prod.* **2018**, 177, 597.
- [84] J. Hong, S. Praver, A. B. Murphy, *ACS Sustain. Chem. Eng.* **2018**, 6(1), 15.
- [85] R. K. Sharma, H. Patel, U. Mushtaq, V. Kyriakou, G. Zafeiropoulos, F. Peeters, S. Welzel, M. C. M. van de Sanden, M. N. Tsampas, *ACS Energy Letters* **2021**, 6(2), 313.
- [86] D. Zhou, R. Zhou, R. Zhou, B. Liu, T. Zhang, Y. Xian, P. J. Cullen, X. Lu, K. Ostrikov, *Chem. Eng. J.* **2021**, 421, 129544. <https://doi.org/10.1016/j.cej.2021.129544>.
- [87] A. George, B. Shen, M. Craven, Y. Wang, D. Kang, C. Wu, X. Tu, *Renew. Sustain. Energ. Rev.* **2021**, 135, 109702. <https://doi.org/10.1016/j.rser.2020.109702>.
- [88] N. García-Moncada, G. van Rooij, T. Cents, L. Lefferts, *Catal. Today* **2021**, 369, 210.
- [89] T. Riyanto, I. Istadi, L. Buchori, D. D. Anggoro, A. B. Dani Nandiyanto, *Ind. Eng. Chem. Res.* **2020**, 59(40), 17632.
- [90] A. Bogaerts, X. Tu, J. C. Whitehead, G. Centi, L. Lefferts, O. Guaitella, F. Azzolina-Jury, H.-H. Kim, A. B. Murphy, W. F. Schneider, T. Nozaki, J. C. Hicks, A. Rousseau, F. Thevenet, A. Khacef, M. Carreon, *J. Phys. D Appl. Phys.* **2020**, 53(44), 443001. <https://doi.org/10.1088/1361-6463/ab9048>.
- [91] M. L. Carreon, *Plasma Research Express* **2019**, 1(4), 43001. <https://doi.org/10.1088/2516-1067/ab5a30>.
- [92] G. Chen, T. Godfroid, N. Britun, V. Georgieva, M.-P. Delplancke-Ogletree, R. Snyders, *Appl. Catal. B-Environ.* **2017**, 214, 114.
- [93] A. Bogaerts, A. Berthelot, S. Heijkers, S. Kolev, R. Snoeckx, S. Sun, G. Trenchev, K. van Laer, W. Wang, *Plasma Sources Sci. T.* **2017**, 26(6), 63001. <https://doi.org/10.1088/1361-6595/aa6ada>.
- [94] I. Tatsuhiko, O. Takashi, O. Tomoyuki, K. Mitsuo, I. Yu, *B. Chem. Soc. Jpn.* **1996**, 69(1), 241.
- [95] P. Mehta, P. Barboun, D. B. Go, J. C. Hicks, W. F. Schneider, *ACS Energy Letters* **2019**, 4(5), 1115.

- [96] K. Ollegott, P. Wirth, C. Oberste-Beulmann, P. Awakowicz, M. Muhler, *Chem.-Ing.-Tech.* **2020**, 92(10), 1542.
- [97] E. C. Neyts, K. Ostrikov, M. K. Sunkara, A. Bogaerts, *Chem. Rev.* **2015**, 115(24), 13408.
- [98] T. Nitsche, C. Unger, E. Weidner, *Chem.-Ing.-Tech.* **2018**, 90(10), 1453.
- [99] N. Bouchoul, H. Touati, E. Fourré, J.-M. Clacens, C. Batiot-Dupeyrat, *Fuel* **2021**, 288, 119575. <https://doi.org/10.1016/j.fuel.2020.119575>.
- [100] E. C. Neyts, A. Bogaerts, *J. Phys. D Appl. Phys.* **2014**, 47(22), 224010. <https://doi.org/10.1088/0022-3727/47/22/224010>.
- [101] S. Liu, L. R. Winter, J. G. Chen, *ACS Catal.* **2020**, 10(4), 2855.
- [102] K. M. Bal, S. Huygh, A. Bogaerts, E. C. Neyts, *Plasma Sources Sci. T.* **2018**, 27(2), 24001. <https://doi.org/10.1088/1361-6595/aaa868>.
- [103] K. M. Bal, E. C. Neyts, *J. Phys. Chem. C* **2019**, 123(10), 6141.
- [104] J. Kruszelnicki, K. W. Engeling, J. E. Foster, M. J. Kushner, *J. Phys. D Appl. Phys.* **2020**, 54(10), 104001. <https://doi.org/10.1088/1361-6463/abcc92>.
- [105] Y. Uytendhouwen, K. M. Bal, I. Michielsen, E. C. Neyts, V. Meynen, P. Cool, A. Bogaerts, *Chem. Eng. J.* **2019**, 372, 1253.
- [106] I. Michielsen, Y. Uytendhouwen, J. Pype, B. Michielsen, J. Mertens, F. Reniers, V. Meynen, A. Bogaerts, *Chem. Eng. J.* **2017**, 326, 477.
- [107] P. Kaliyappan, A. Paulus, J. D'Haen, P. Samyn, Y. Uytendhouwen, N. Hafezkhiani, A. Bogaerts, V. Meynen, K. Elen, A. Hardy, M. K. van Bael, *J. CO₂ Util.* **2021**, 46, 101468. <https://doi.org/10.1016/j.jcou.2021.101468>.
- [108] Y. Uytendhouwen, V. Meynen, P. Cool, A. Bogaerts, *Catalysts* **2020**, 10(5), 530. <https://doi.org/10.3390/catal10050530>.
- [109] A. Bloess, W.-P. Schill, A. Zerrahn, *Appl. Energ.* **2018**, 212, 1611.
- [110] V. Vasiliev, E. Morozov, *Advanced Mechanics of Composite Materials and Structures*, 4th ed., Elsevier, Amsterdam, The Netherlands **2018**.
- [111] F. Lux, *J. Mater. Sci.* **1993**, 28, 285.
- [112] S. H. Ryu, H.-B. Cho, S. Kim, Y.-T. Kwon, J. Lee, K.-R. Park, Y.-H. Choa, *Compos. Sci. Technol.* **2018**, 165, 1.
- [113] V. Schallhart, H. Berthold, E. Klemm, L. Moeltner, *Chem.-Ing.-Tech.* **2021**, 93(5), 814.
- [114] G. Takalkar, R. R. Bhosale, F. AlMomani, M. Khraisheh, *Fuel* **2019**, 257, 115965. <https://doi.org/10.1016/j.fuel.2019.115965>.
- [115] W. Jin, C. Zhang, P. Zhang, Y. Fan, N. Zu, *AIChE J.* **2006**, 52(7), 2545. <https://doi.org/10.1002/aic.10850>.
- [116] R. C. Pullar, R. M. Novais, A. P. F. Caetano, M. A. Barreiros, S. Abanades, F. A. C. Oliveira, *Front. Chem.* **2019**, 7, 601.
- [117] R. R. Bhosale, A. Kumar, F. AlMomani, U. Ghosh, P. Sutar, G. Takalkar, A. Ashok, I. Alxneit, *Ceram. Int.* **2017**, 43(6), 5150.
- [118] M. Kang, J. Zhang, N. Zhao, W. Wei, Y.-H. Sun, *Journal of Fuel Chemistry and Technology* **2014**, 42(1), 68.
- [119] J. Toyir, R. Miloua, N. E. Elkadri, M. Nawdali, H. Toufik, F. Miloua, M. Saito, *Physcs. Proc.* **2009**, 2(3), 1075.
- [120] X. Wang, H. Shi, J. H. Kwak, J. Szanyi, *ACS Catal.* **2015**, 5(11), 6337.
- [121] H. Kusama, K. K. Bando, K. Okabe, H. Arakawa, *Appl. Catal. A-Gen.* **2001**, 205(1), 285.
- [122] B. Lu, Y. Ju, T. Abe, K. Kawamoto, *Inorg. Chem. Front.* **2015**, 2(8), 741.
- [123] M. D. Porosoff, X. Yang, J. A. Boscoboinik, J. G. Chen, *Angew Chem. Int. Edit.* **2014**, 53(26), 6705.
- [124] S. Roy, A. Cherevotan, S. C. Peter, *ACS Energy Letters* **2018**, 3(8), 1938.
- [125] Technology Readiness Levels Demystified, https://www.nasa.gov/topics/aeronautics/features/trl_demystified.html (accessed: July 2021).
- [126] A. W. Zimmermann, G. A. Buchner, R. Schomäcker, *Energy Technol.-Ger.* **2021**, 9(2), 2000691. <https://doi.org/10.1002/ente.202000691>
- [127] C. Zhu, S. Hou, X. Hu, J. Lu, F. Chen, K. Xie, *Nat. Commun.* **2019**, 10(1), 1173.
- [128] V. Kyriakou, C. Athanasiou, I. Garagounis, A. Skodra, M. Stoukides, *Int. J. Hydrogen Energ.* **2012**, 37(21), 16636.
- [129] H. Yang, J. J. Kaczur, S. D. Sajjad, R. I. Masel, *J. CO₂ Util.* **2020**, 42, 101349. <https://doi.org/10.1016/j.jcou.2020.101349>.
- [130] Z. Liu, H. Yang, R. Kutz, R. I. Masel, *J. Electrochem. Soc.* **2018**, 165(15), J3371.
- [131] I. Yamanaka, T. Hashimoto, R. Ichihashi, K. Otsuka, *Electrochim. Acta* **2008**, 53(14), 4824.
- [132] A. J. Martín, G. O. Larrazábal, J. Pérez-Ramírez, *Green Chem.* **2015**, 17(12), 5114.
- [133] B. J. M. Etzold, U. Krewer, S. Thiele, A. Dreizler, E. Klemm, T. Turek, *Chem. Eng. J.* **2021**, 424, 130501. <https://doi.org/10.1016/j.cej.2021.130501>.
- [134] R. Küngas, *J. Electrochem. Soc.* **2020**, 167(4), 44508. <https://doi.org/10.1149/1945-7111/ab7099>.
- [135] R. Küngas, P. Blennow, T. Heiredal-Clausen, T. Holt, J. Rass-Hansen, S. Primdahl, J. B. Hansen, *ECS Transactions* **2017**, 78(1), 2879.
- [136] M. P. Heddrich, S. Gupta, S. Santhanam, *Chem.-Ing.-Tech.* **2019**, 91(6), 809.
- [137] V. Kyriakou, I. Garagounis, E. Vasileiou, A. Vourros, M. Stoukides, *Catal. Today* **2017**, 286, 2.
- [138] A. Ozkan, T. Dufour, T. Silva, N. Britun, R. Snyders, A. Bogaerts, F. Reniers, *Plasma Sources Sci. T.* **2016**, 25(2), 25013. <https://doi.org/10.1088/0963-0252/25/2/025013>.
- [139] J.-L. Liu, X. Wang, X.-S. Li, B. Likozar, A.-M. Zhu, *J. Phys. D Appl. Phys.* **2020**, 53, 253001. <https://doi.org/10.1088/1361-6463/ab7c04>.
- [140] H. Wirth, *Recent Facts about Photovoltaics in Germany*, Fraunhofer Institute, Freiburg, Germany **2021**.
- [141] Suez Water Technologies & Solutions Ozonia Ozone Generator Systems for Water Treatment, <https://www.suezwatertech.com/products/disinfection-oxidation/ozonia-ozone-systems> (accessed: August 2021).

SUPPORTING INFORMATION

Additional supporting information may be found in the online version of the article at the publisher's website.

How to cite this article: E. Klemm, C. M. S. Lobo, A. Löwe, V. Schallhart, S. Renninger, L. Waltersmann, R. Costa, A. Schulz, R.-U. Dietrich, L. Möltner, V. Meynen, A. Sauer, K. A. Friedrich, *Can. J. Chem. Eng.* **2022**, 100(10), 2736. <https://doi.org/10.1002/cjce.24397>